ADAPTIVE DISCRETE-ORDINATES ALGORITHMS AND STRATEGIES

A Dissertation

by

JOSEPH CARLYLE STONE

Submitted to the Office of Graduate Studies of
Texas A&M University
in partial fulfillment of the requirements for the degree of

DOCTOR OF PHILOSOPHY

December 2007

Major Subject: Nuclear Engineering

ADAPTIVE DISCRETE-ORDINATES ALGORITHMS AND STRATEGIES

A Dissertation

by

JOSEPH CARLYLE STONE

Submitted to the Office of Graduate Studies of
Texas A&M University
in partial fulfillment of the requirements for the degree of

DOCTOR OF PHILOSOPHY

Approved by:

Chair of Committee,	Marvin L. Adams
Committee Members,	Raytcho Lazarov
	Jim E. Morel
	Paul Nelson
	Jean C. Ragusa
Head of Department,	John W. Poston Sr.

December 2007

Major Subject: Nuclear Engineering

ABSTRACT

Adaptive Discrete-Ordinates Algorithms and Strategies. (December 2007)

Joseph Carlyle Stone, B.S., Texas A&M University; M.S., Texas A&M University

Chair of Advisory Committee: Dr. Marvin L. Adams

The approaches for discretizing the direction variable in particle transport calculations are the discrete-ordinates method and function-expansion methods. Both approaches are limited if the transport solution is not smooth.

Angular discretization errors in the discrete-ordinates method arise from the inability of a given quadrature set to accurately perform the needed integrals over the direction ("angular") domain. We propose that an adaptive discrete-ordinate algorithm will be useful in many problems of practical interest. We start with a "base quadrature set" and add quadrature points as needed in order to resolve the angular flux function. We compare an interpolated angular-flux value against a calculated value. If the values are within a user specified tolerance, the point is not added; otherwise it is. Upon the addition of a point we must recalculate weights.

Our interpolatory functions map angular-flux values at the quadrature directions to a continuous function that can be evaluated at any direction. We force our quadrature weights to be consistent with these functions in the sense that the quadrature integral of the angular flux is the exact integral of the interpolatory function (a finite-element

methodology that determines coefficients by collocation instead of the usual weighted-residual procedure).

We demonstrate our approach in two-dimensional Cartesian geometry, focusing on the azimuthal direction The interpolative methods we test are simple linear, linear in sine and cosine, an Abu-Shumays "base" quadrature with a simple linear adaptive and an Abu-Shumays "base" quadrature with a linear in sine and cosine adaptive. In the latter two methods the local refinement does not reduce the ability of the base set to integrate high-order spherical harmonics (important in problems with highly anisotropic scattering).

We utilize a variety of one-group test problems to demonstrate that in all cases, angular discretization errors (including "ray effects") can be eliminated to whatever tolerance the user requests. We further demonstrate through detailed quantitative analysis that local refinement does indeed produce a more efficient placement of unknowns.

We conclude that this work introduces a very promising approach to a long-standing problem in deterministic transport, and we believe it will lead to fruitful avenues of further investigation.

DEDICATION

I would like to dedicate this work to my loving wife, Hiromi. It is by her inspiration and motivating influence that I have completed this work.

ACKNOWLEDGEMENTS

I would like to thank my committee chair, Dr. Adams, and my committee members, Dr. Lazarov, Dr. Morel, Dr. Nelson, and Dr. Ragusa, for their guidance and support throughout the course of this research.

Thanks also go to my friends and colleagues and the department faculty and staff for making my time at Texas A&M University a great experience. I also want to thank the US DOE Nuclear Engineering Educational Research (NEER) Program, which partially funded this research.

I would also like to acknowledge and thank Jerome Truax for letting me stay on at Halliburton as an intern while I finished; and of course Weijun Guo and Prakash Hanagud who patiently listened to my endless troubles and theories.

Finally, thanks to my mother, father, and sister for their encouragement and to my wife and children for their patience and love.

TABLE OF CONTENTS

LIST OF FIGURES

I. INTRODUCTION: ANGULAR DISCRETIZATION ERRORS

A. Introduction

The angular discretization errors inherent in the deterministic solutions of transport are a major problem.[1] Angular discretization errors, including ray effects, severely limit the use of discrete ordinate methods. They arise from quadrature-rule limitations (see Section 3). The example shown below (constructed to make it relatively easy to solve analytically) illustrates how ray effects distort the correct answer and motivates the adaptive discrete ordinate algorithms we present in this dissertation.

B. Motivation

Figure 1 shows a two-dimensional problem containing a circular isotropic source centered at the origin in a non-scattering material of uniform composition. The exact scalar flux in our example problem is the same at points A and B, since A and B are exactly the same distance from the source (r units). Figure 2 is the plot of the angular flux (at the distance, r from the center of the source) for both points A and B as a function of the azimuthal direction. For the moment we ignore the variation of the angular flux (ψ) in the polar angle, θ.

_____

This dissertation follows the style and format of *Nuclear Science and Engineering.*
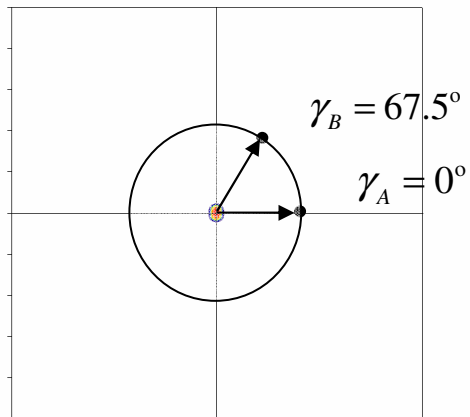
Figure 1   A circular isotropic source in a purely absorbing medium.
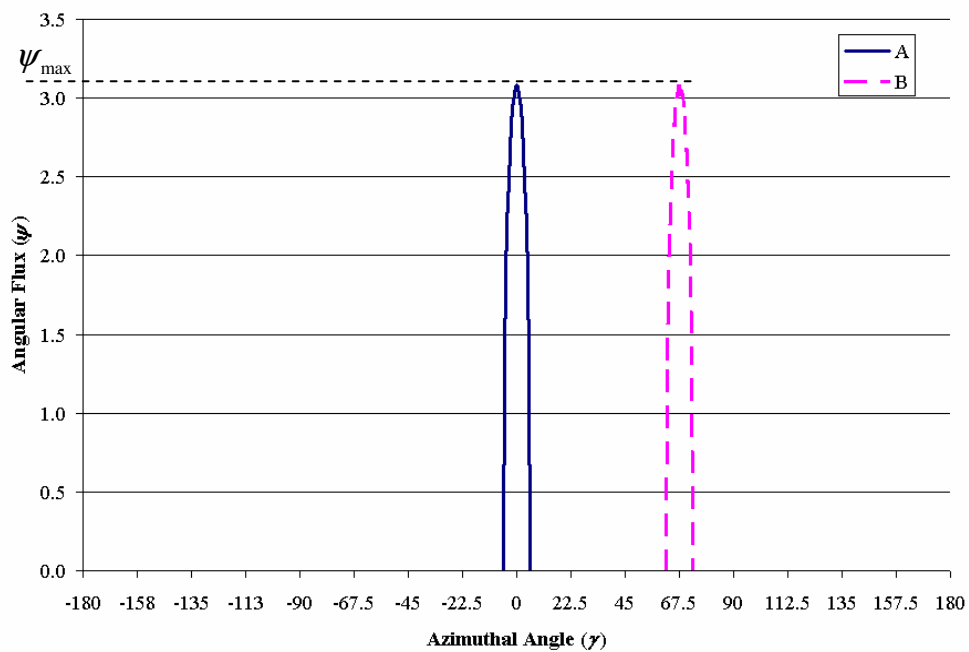
Figure 2   This figure displays angular flux as a function of azimuthal direction γ for points A and B, at an arbitrary polar angle.

Suppose we use the discrete ordinates method (see Section 2) with a coarse

quadrature set of 8 equally spaced quadrature points in the azimuthal variable (γ) to

solve for the scalar flux (ϕ) at points A and B. The quadrature points are at

$\gamma = -157.5°$, $-112.5°$, $-72.5°$, $-22.5°$, $22.5°$, $67.5°$, $112.5°$ and $157.5°$. Each of the

quadrature weights (w_m) has the same value $\left(\dfrac{\pi}{4}\right)$. The scalar flux approximation at

points A and B are

$$\phi_A \approx \frac{\pi}{4}\sum_{m=1}^{8}\psi_A\left(\gamma_m\right) = 0 \tag{1.1}$$

and

$$\phi_B \approx \frac{\pi}{4}\sum_{m=1}^{8}\psi_B\left(\gamma_m\right) = \frac{\pi}{4}\psi_{max} \tag{1.2}$$

respectively. As this example illustrates, the angular-flux functions, which are not

smooth, are very difficult to integrate with accuracy if only a single quadrature set is

used.

If we plot the scalar flux (calculated using this coarse quadrature set) along a circle

centered on the source, the plot will oscillate between zero (in the positions between the

angles in our quadrature set) and values that are much larger than that of the correct

scalar flux (near positions that correspond to the angles in our quadrature set). The true

scalar flux is constant along the circle. Figure 3 shows a pseudo-color plot of scalar flux

for this problem using the coarse quadrature set.
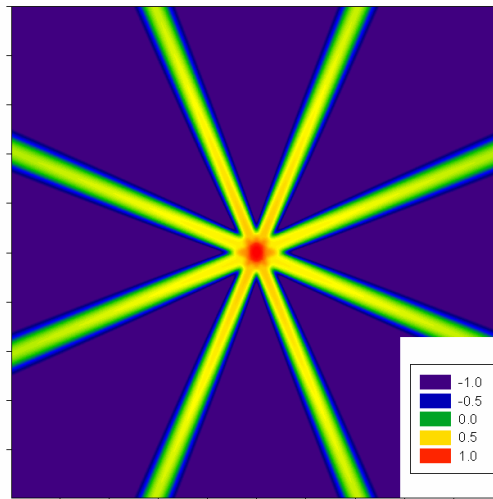
Figure 3   A pseudo-color plot of the logarithm of the scalar flux using the 8-point quadrature set in the discrete-ordinates approximation. The values in the legend are powers of 10.

Ray effects are unphysical oscillations in the scalar flux. They are caused by the inability of a quadrature set in the discrete-ordinates approximation to accurately integrate the angular flux. If the spatial locations of the points of interest are sufficiently far enough from the source, it is not difficult to see that any fixed finite quadrature set will suffer from ray effects. In the example, points closer to the source than A and B have wider peaks. Therefore their scalar flux can be more accurately approximated with a coarser quadrature set (i.e. relatively few abscissae are needed to accurately integrate the peaks as one moves closer to the source). However, as one looks farther from the source, the peaks of angular flux become narrower and more difficult to integrate with a coarse quadrature set. To summarize, ray effects occur when the discrete ordinates quadrature set integrates two functions differently even though one is just a translation (in angle) of the other. Ray effects are most pronounced when the angular flux oscillates significantly as a function of angle (i.e., is a "peaky" function).

If the quadrature set were allowed to conform to the solution at any spatial point of interest, the example problem that we have illustrated above could be accurately integrated with very little effort. This would require only that the abscissas in the quadrature set be "properly placed."

C. Related Works

The simplest approach to mitigating ray effects is to increase the number of points (size) of the quadrature set. This approach will cause the frequency of ray-effect oscillations to increase and the magnitude to become smaller.[2] Even so, the ray effects can be persistent, as mentioned in the example above and as shown by K. D. Lathrop.[3]

Another class of methods used to mitigate the ray effects is to use piecewise continuous function expansions to approximate the angular dependence of the angular flux. Equations for the coefficients are usually obtained by weighting and integrating the transport equation over the angular domain.[4] These methods are sometimes called angularly smeared methods. Examples include spherical-harmonics ("P_N") methods, quadruple (2D) or octuple (3D) P_N methods,[5,6,7] and finite element methods.[8] While all of these methods can mitigate ray effects to some extent, only the full P_N method eliminates them. In addition, all of these methods (including full P_N) suffer from persistent angular discretization errors as the number of unknowns increases. The root of the difficulty is that the angular flux in a realistic problem is far from smooth and thus is not well approximated by smooth or piecewise-smooth functions that are chosen in advance (as opposed to adapted to the local solution).

Another method that helps with the problem of ray effects is to compute analytically the un-collided flux then use this to generate a first-collision source. While the analytic first-collision source is a good and helpful thing to do, it does not solve the problem of ray effects or other angular discretization errors.

Another approach, which still utilizes discrete ordinates, is to locally refine a quadrature set to provide a large number of quadrature points in one or more directional cones.[9,10] Production codes DORT (2-D)[11] and TORT (3-D),[12] developed at Oak Ridge National Laboratory, can utilize region-dependent cross sections. An example of where this approach is useful would be problems having a localized source and a localized region of interest (such as a detector). This approach is one type of locally refined discrete ordinate method, but it is user-controlled as opposed to adaptive. We propose that a truly adaptive discrete ordinate algorithm (as in the generalized description that we outlined at the beginning of this section) will be useful in more general problems.

D. Objectives

In this dissertation we develop and test algorithms for adapting (refining) discrete ordinate quadrature sets to solve two-dimensional Cartesian-geometry particle transport problems. We show that it is possible to eliminate ray effects and other angular discretization errors by refinement of the quadrature set locally in both position and direction. By appropriate refinement we resolve angular variations in the angular flux through the efficient placement of new quadrature abscissas in order to accurately integrate the angular flux. We divide the problem spatial domain into "quadrature

regions" with different quadrature sets allowed in different regions. We assume a polar quadrature set (adaptable in principle) and an azimuthal set that can adapt independently on each polar level. The use of locally adapted quadrature sets makes it possible to reduce the unknown count required to achieve a given accuracy, compared to the use of any single quadrature set across the spatial domain.

In Section 2 we review the derivation of the two-dimensional, one-speed, time-independent neutral-particle transport equation, including a brief overview of eigenvalue problems that arise in neutron transport. We discuss the usual ways that the transport equation is discretized in time, energy, space and direction. In Section 3 we review various quadrature rules, some of which we use to create our starting quadrature sets before we begin adapting. In Section 4 we discuss the methods we have created for our adaptive algorithms. We also explain our method for enforcing particle conservation. In Section 5 we give a brief outline of our program's algorithm. We describe our test problems and our numerical results. We also present our analysis of the numerical results. Section 6 comprises our conclusions on the work presented herein and outlines some of the prospects we envision for future work in this area.

II. PROBLEM DEFINITIONS

A. Boltzmann Transport Equation

The time-dependent linear Boltzmann transport equation for particles is:[4]

$$\frac{1}{\mathrm{v}(E)}\frac{\partial}{\partial t}\psi\left(\bar{r},\bar{\Omega},E,t\right)+\bar{\Omega}{\cdot}\bar{\nabla}\,\psi\left(\bar{r},\bar{\Omega},E,t\right)+\Sigma_{t}\left(\bar{r},E,t\right)\psi\left(\bar{r},\bar{\Omega},E,t\right)$$
$$= S\left(\bar{r},\bar{\Omega},E,t\right),$$

(2.1)

where the angular flux $\psi\left(\bar{r},\bar{\Omega},E,t\right)$ is a function of energy (E), position

$\left(\bar{r}\equiv f\left(x,y,z\right)\right)$, direction $\left(\bar{\Omega}\equiv f\left(\gamma,\theta\right)\right)$ and time (t). The speed of a particle with

kinetic energy (E) is $\mathrm{v}(E)$; $\Sigma_{t}\left(\bar{r},E\right)$ is the total collision cross section; and

$S\left(\bar{r},\bar{\Omega},E,t\right)$ is the total source rate density, including scattering, fission and fixed

sources. The transport equation is a conservation equation or balance equation. It simply

states that the "rate of change" plus the "rate of loss" equals the "rate of gain," and it

models the behavior of particles in seven dimensions.

We limit the focus of this work to neutral particles. There are fundamental

assumptions that are made in order to derive the neutral particle transport equation:

particles are considered to be points; particles travel in straight lines between collisions;

there are no particle-particle interactions; the material properties of the medium in which

the particles exist are considered isotropic; and only the mean value of particle density is considered.[13]

B. Source Term

The source term of the particle transport equation is divided into three sub-terms, the external source rate density, the fission source rate density (if the particles are neutrons), and the in-scattering rate density:

$$
\begin{aligned}
S\left(\vec{r},\bar{\Omega},E,t\right) \\
= S_{ext}\left(\vec{r},\bar{\Omega},E,t\right) + \frac{\chi(E)}{4\pi}\int_0^\infty dE'\upsilon\Sigma_f\left(\vec{r},E',t\right)\int_{4\pi} d\Omega'\psi\left(\vec{r},\Omega',E',t\right) \\
+ \int_{4\pi} d\Omega'\int_0^\infty dE'\psi\left(\vec{r},\bar{\Omega}',E',t\right)\Sigma_s\left(\vec{r},\bar{\Omega}'\to\Omega,E'\to E,t\right).
\end{aligned}
\tag{2.2}
$$

The external source rate density $\left(S_{ext}\right)$ is the rate of particle emission into the six-dimensional (energy, position and direction) phase volume. It is independent of particle density. The next term is the gain from fission. The energy spectrum, $\chi(E)$ is a probability function:

$$
\int_0^\infty \chi(E)dE = 1
\tag{2.3}
$$

It represents the distribution of neutrons born from fission into the energy dimension of phase volume. These neutrons are born in an isotropic manner. The mean number of neutrons produced from a fission into the phase volume caused by a neutron of energy E' is $v(\bar{r}, E', t)$. The macroscopic fission cross section is $\Sigma_f(\bar{r}, E', t)$. Since v is always multiplied by Σ_f, they are normally denoted as a single variable $v\Sigma_f$.[11] The direction integration of the fission term is simplified by using the definition of scalar flux:

$$\phi(\bar{r}, E, t) = \int_{4\pi} d\bar{\Omega}\, \psi(\bar{r}, \bar{\Omega}, E, t) \tag{2.4}$$

The last term is the gain due to in-scattering of particles into the energy and direction dimensions of phase volume. The composite differential scattering cross sections (Σ_s) is a combination of the scattering cross sections and scattering distributions of many different materials. This combination is written in the following short-hand:

$$\Sigma_s\left(\bar{r}, E \rightarrow E', \bar{\Omega} \rightarrow \bar{\Omega}'\right) = \sum_i \Sigma_s^i\left(\bar{r}, E \rightarrow E', \bar{\Omega} \rightarrow \bar{\Omega}'\right) \tag{2.5}$$

Each nuclide in a mixture (denoted by i) has its own scattering cross section and scattering distribution. We insert the source terms into Eq. (2.1) to produce the time dependent transport equation that treats delayed neutrons as part of the external source:

$$\frac{1}{v}\frac{\partial}{\partial t}\psi\left(\bar{r},\bar{\Omega},E,t\right)+\bar{\Omega}\cdot\bar{\nabla}\psi\left(\bar{r},\bar{\Omega},E,t\right)+\Sigma_t\left(\bar{r},E,t\right)\psi\left(\bar{r},\bar{\Omega},E,t\right)$$

$$=S_{ext}\left(\bar{r},\bar{\Omega},E,t\right)+\frac{\chi(E)}{4\pi}\int_0^\infty dE'\phi\left(\bar{r},E',t\right)v\Sigma_f\left(\bar{r},E',t\right) \qquad (2.6)$$

$$+\int_{4\pi}d\Omega'\int_0^\infty dE'\psi\left(\bar{r},\bar{\Omega}',E',t\right)\Sigma_s\left(\bar{r},\bar{\Omega}'\rightarrow\Omega,E'\rightarrow E,t\right).$$

If the particles are not neutrons the fission term is omitted.

C. The α and k Eigenvalue Problems

The physical definition of a critical system is a system capable of maintaining a self-sustaining, time-independent chain reaction in the absence of an external source of neutrons. In other words, it is a system that exists in equilibrium, with the number of neutrons produced from fission equal to the number of neutrons that are absorbed or leak from the system.[4] If the system cannot maintain equilibrium, the asymptotic population of neutrons (the fundamental mode) will either increase (super-critical) or decrease (sub-critical) with time exponentially. In the presence of an external source of neutrons, a sub-critical system will eventually come to a state of equilibrium (i.e. the production of the external and fission neutrons is balanced by the absorption and leakage from the system). A critical or super-critical system cannot maintain equilibrium with the presence of an external source and the neutron flux distribution will be an increasing function of time. If a system is critical it has a nonnegative solution to the time

independent source free transport equation with appropriate boundary conditions.[4] The

time-independent form suppresses the time argument of Eq (2.6):

$$
\left[\bar{\Omega}\bullet\bar{\nabla}+\Sigma_t\left(\bar{r},E\right)\right]\psi\left(\bar{r},\bar{\Omega},E\right)=S_{ext}\left(\bar{r},\bar{\Omega},E,t\right)+
$$
$$
\int d\Omega'\int dE'\psi\left(\bar{r},\bar{\Omega}',E'\right)\Sigma_s\left(\bar{r},\bar{\Omega}'\to\Omega,E'\to E\right) \quad (2.7)
$$
$$
+\frac{\chi(E)}{4\pi}\int dE' v\Sigma_f\left(\bar{r},E'\right)\phi\left(\bar{r},E'\right), \quad \bar{r}\in V.
$$

This is accompanied by appropriate boundary conditions, such as

$$
\psi\left(\bar{r},\bar{\Omega},E\right)=0 \quad \bar{n}\bullet\bar{\Omega}<0, \bar{r}\in\Gamma, \quad (2.8)
$$

where V is the volume of the system and Γ is its surface. If a system is sub-critical then

there exists a solution to the time-independent transport equation with a non-zero fixed

external source:

$$
\left[\bar{\Omega}\bullet\bar{\nabla}+\Sigma_t\left(\bar{r},E\right)\right]\psi\left(\bar{r},\bar{\Omega},E\right)=S_{ext}\left(\bar{r},\bar{\Omega},E\right)
$$
$$
+\int d\Omega'\int dE'\psi\left(\bar{r},\bar{\Omega}',E'\right)\Sigma_s\left(\bar{r},\bar{\Omega}'\to\Omega,E'\to E\right) \quad (2.9)
$$
$$
+\frac{\chi(E)}{4\pi}\int dE' v\Sigma_f\left(\bar{r},E'\right)\int d\Omega\psi\left(\bar{r},E',\bar{\Omega}\right), \quad \bar{r}\in V,
$$

where there is a known distribution of neutrons entering the system across its surface:

$$\psi\left(\bar{r},\bar{\Omega},E\right)=\Psi\left(\bar{r},\bar{\Omega}\right) \quad \bar{n}\bullet\bar{\Omega}<0, \bar{r}\in\Gamma. \tag{2.10}$$

Eigenvalue problems tell us how a system would behave in the absence of any "forcing" (in our case sources and incident fluxes) if they were left alone. The time-absorption eigenvalue calculation $\left(\alpha-\text{eigenvalue}\right)$ is one of the options found in most discrete-ordinates transport codes.[13] It presents a solution of the transport equation in the form of a constant angular flux times an exponential. The $\alpha-\text{eigenvalue}$ problem looks for solutions to Eq. (2.7) that take the form:

$$\psi\left(\bar{r},\bar{\Omega},E,t\right)=\psi_{\alpha}\left(\bar{r},\bar{\Omega},E\right)e^{\alpha t}, \tag{2.11}$$

and satisfy the boundary conditions (2.8). We insert Eq. (2.11) into Eq. (2.7)and set the external source to zero:

$$\left[\bar{\Omega}\bullet\bar{\nabla}+\Sigma_{t}\left(\bar{r},E\right)+\frac{\alpha}{v}\right]\psi_{\alpha}\left(\bar{r},\bar{\Omega},E\right)=\int d\Omega'\int dE'\psi_{\alpha}\left(\bar{r},\bar{\Omega}',E'\right)\Sigma_{s}\left(\bar{r},\bar{\Omega}'\bullet\Omega,E'\rightarrow E\right)$$
$$+\frac{\chi(E)}{4\pi}\int dE'v\Sigma_{f}\left(\bar{r},E'\right)\int d\Omega\psi_{\alpha}\left(\bar{r},E',\bar{\Omega}\right), \quad \bar{r}\in V \tag{2.12}$$

If a system is left on its own for a long time , then the angular flux will take the shape of the eigenfunction corresponding to the α with the largest real part (α_{0}). If α_{0}

is positive then the system is supercritical; if α_0 is negative then the system is sub-

critical; and if α_0 is zero then the system is critical.

The k-eigenvalue calculations are made to ascertain the neutron multiplication factor. The *k*-eigenvalue problem replaces the average number of neutrons per fission (v) with

$\dfrac{v}{k}$. The physical interpretation is that v can be adjusted such that a solution to Eq. (2.7)

exists:

$$\left[\vec{\Omega}\bullet\vec{\nabla}+\Sigma_t\left(\vec{r},E\right)\right]\psi\left(\vec{r},\vec{\Omega},E\right)=\int d\Omega'\int dE'\psi\left(\vec{r},\vec{\Omega}',E'\right)\Sigma_s\left(\vec{r},\vec{\Omega}'\to\Omega,E'\to E\right)$$
$$+\frac{\chi(E)}{k4\pi}\int dE'v\Sigma_f\left(\vec{r},E'\right)\int d\Omega\,\psi\left(\vec{r},E',\vec{\Omega}\right),\quad \vec{r}\in V.$$

(2.13)

Any chain reaction system with a non-zero $v\Sigma_f$ can be made critical by such an

adjustment.[4] There will always be a largest eigenvalue, k, for which the associated

eigenfunction, ψ, is non-negative. If this value of k is greater than one then the system

is super-critical; if it is one then the system is critical; if it is less than one the system is

sub-critical. Solutions to the *k*-eigenvalue equation are often found using power iteration.

D. Discretization in Time

We do not analyze time-dependent problems in this research. We provide a brief

discussion of discretization in time only to give a perspective of the benefits an adaptive

algorithm may have in time-dependent problems. Finite-differencing the derivative in time is the approach most often taken. The exact equations are integrated over the time step $\Delta t = t_n - t_{n-1}$ and functions are denoted with an over-bar to indicate they are averages over the time step:

$$\bar{\psi}\left(\bar{r},\bar{\Omega},E\right)=\frac{1}{\Delta t}\int\limits_{t_{n-1}}^{t_n} dt\psi\left(\bar{r},\bar{\Omega},E,t\right) \tag{2.14}$$

$$\bar{S}_{ext}\left(\bar{r},E\right)=\frac{1}{\Delta t}\int\limits_{t_{n-1}}^{t_n} dt S_{ext}\left(\bar{r},\bar{\Omega},E,t\right) \tag{2.15}$$

We lump the fission term into our external source term $\left(S_{ext}\right)$ and substitute the average definitions (Eqs. (2.14) and (2.15)) into Eq. 2.6 to form the time difference equation:

$$\frac{\psi_n\left(\bar{r},\bar{\Omega},E\right)-\psi_{n-1}\left(\bar{r},\bar{\Omega},E\right)}{v\Delta t}+\bar{\Omega}\bullet\bar{\nabla}\,\bar{\psi}\left(\bar{r},\bar{\Omega},E\right)+\Sigma_t\left(\bar{r},E\right)\bar{\psi}\left(\bar{r},\bar{\Omega},E\right)=$$
$$\bar{S}_{ext}\left(\bar{r},\bar{\Omega},E\right)+\int\limits_{0}^{\infty}dE'\int\limits_{4\pi}d\Omega'\Sigma_s\left(\bar{r},\bar{\Omega}'\rightarrow\Omega,E'\rightarrow E\right)\bar{\psi}\left(\bar{r},\bar{\Omega}',E'\right) \tag{2.16}$$

$\psi_{n-1}\left(\bar{r},\bar{\Omega},E\right)$ is known from the previous time step; however $\psi_n\left(\bar{r},\bar{\Omega},E\right)$ and $\bar{\psi}\left(\bar{r},\bar{\Omega},E\right)$ are not known. The simplest solution is to assume a relationship among the three, such as:

$$\bar{\psi}\left(\bar{r},\bar{\Omega},E\right)=\beta\psi_n\left(\bar{r},\bar{\Omega},E\right)+\left(1-\beta\right)\psi_{n-1}\left(\bar{r},\bar{\Omega},E\right) \tag{2.17}$$

We use Eq. (2.17) to eliminate $\psi_n\left(\bar{r},\bar{\Omega},E\right)$ from Eq. (2.16):

$$\bar{\Omega}\bullet\bar{\nabla}\,\bar{\psi}\left(\bar{r},\bar{\Omega},E\right)+\left(\Sigma_t\left(\bar{r},E\right)+\frac{1}{\beta v\Delta t}\right)\bar{\psi}\left(\bar{r},\bar{\Omega},E\right)=\left(\bar{S}_{ext}\left(\bar{r},\bar{\Omega},E\right)+\frac{\psi_{n-1}\left(\bar{r},\bar{\Omega},E\right)}{\beta v\Delta t}\right)$$

$$+\int_0^\infty dE'\int_{4\pi} d\Omega'\Sigma_s\left(\bar{r},\bar{\Omega}'\to\Omega,E'\to E\right)\bar{\psi}\left(\bar{r},\bar{\Omega}',E'\right) \tag{2.18}$$

We now solve a series of steady state problems (one per time step) with an "effective" total cross section and an "effective" source. We eliminate the over-bars and combine the terms within brackets:

$$\left(\bar{S}_{ext}\left(\bar{r},\bar{\Omega},E\right)+\frac{\psi_{n-1}\left(\bar{r},\bar{\Omega},E\right)}{\beta v\Delta t}\right)\to S_{ext}\left(\bar{r},\bar{\Omega},E\right); \tag{2.19}$$

and

$$\left(\Sigma_t\left(\bar{r},E\right)+\frac{1}{\beta v\Delta t}\right)\to\Sigma_t\left(\bar{r},E\right). \tag{2.20}$$

Eq. (2.18) can now be written as a time-independent equation:

$$\bar{\Omega}\cdot\bar{\nabla}\psi\left(\bar{r},\bar{\Omega},E\right)+\Sigma_t\left(\bar{r},E\right)\psi\left(\bar{r},\bar{\Omega},E\right)=$$

$$S_{ext}\left(\bar{r},\bar{\Omega},E\right)+\int\limits_0^\infty dE'\int\limits_{4\pi}d\Omega'\Sigma_s\left(\bar{r},\bar{\Omega}'\to\Omega,E'\to E\right)\psi\left(\bar{r},\bar{\Omega}',E'\right). \tag{2.21}$$

E. Discretization in Energy

The multi-group approximation to discretize the energy variable divides the energy range of the particles into G intervals with $E_G = 0$ and E_0 sufficiently large such that the number of particles with energies above E_0 is insignificant. The particles in group g are defined as particles with energies greater than E_g and less than E_{g-1}. The objective here is to obtain an approximation to the transport equation in terms of the group angular flux:[4]

$$\psi_g\left(\bar{r},\bar{\Omega}\right)=\int\limits_{E_g}^{E_{g-1}}dE\psi\left(\bar{r},\bar{\Omega},E\right)=\int\limits_g^{g-1}dE\psi\left(\bar{r},\bar{\Omega},E\right) \tag{2.22}$$

Now divide the energy integral in Eq. (2.22) into the contributions from each energy group:

$$\bar{\Omega}\cdot\bar{\nabla}\psi\left(\bar{r},\bar{\Omega},E\right)+\Sigma_t\left(\bar{r},E\right)\psi\left(\bar{r},\bar{\Omega},E\right)=S_{ext}\left(\bar{r},\bar{\Omega},E\right)$$

$$+\sum_{g'=1}^{G}\int\limits_{g'}^{g'-1}dE'\int\limits_{4\pi}d\Omega'\Sigma_s\left(\bar{r},\bar{\Omega}'\to\Omega,E'\to E\right)\psi\left(\bar{r},\bar{\Omega}',E'\right). \tag{2.23}$$

Then integrate over the energy range E_g to E_{g-1}:

$$\vec{\Omega}\cdot\vec{\nabla}\int_g^{g-1} dE\psi\left(\vec{r},\vec{\Omega},E\right)+\int_g^{g-1} dE\Sigma_t\left(\vec{r},E\right)\psi\left(\vec{r},\vec{\Omega},E\right)=\int_g^{g-1} dES_{ext}\left(\vec{r},\vec{\Omega},E\right)$$

$$+\int_g^{g-1} dE\sum_{g'=1}^{G}\int_{g'}^{g'-1} dE'\int_{4\pi} d\Omega'\Sigma_s\left(\vec{r},\vec{\Omega}'\to\Omega,E'\to E\right)\psi\left(\vec{r},\vec{\Omega}',E'\right). \tag{2.24}$$

Next define *group source* as follows:

$$S_g\left(\vec{r},\vec{\Omega}\right)\equiv\int_g^{g-1} dES_{ext}\left(\vec{r},\vec{\Omega},E\right) \tag{2.25}$$

The next step is to assume a shape function in energy (an energy spectrum) and use it in place of the exact solution ψ to obtain group-averaged cross sections. This is called the spectrum "f" and the multi-group approximation is:

$$\frac{\int_g^{g-1} dE\Sigma_t\left(\vec{r},E\right)\psi\left(\vec{r},\vec{\Omega},E\right)}{\int_g^{g-1} dE\psi\left(\vec{r},\vec{\Omega},E\right)}\to\frac{\int_g^{g-1} dE\Sigma_t\left(\vec{r},E\right)f\left(\vec{r},E\right)}{\int_g^{g-1} dEf\left(\vec{r},E\right)}\equiv\Sigma_{tg}\left(\vec{r}\right), \tag{2.26}$$

(f is usually assumed to be independent of direction) and

$$\frac{\displaystyle\int_{g'}^{g'-1} dE' \left[\int_{g}^{g-1} dE \Sigma_s \left(\vec{r}, \bar{\Omega}' \to \Omega, E' \to E \right) \right] \psi \left(\vec{r}, \bar{\Omega}', E' \right)}{\displaystyle\int_{g'}^{g'-1} dE' \psi \left(\vec{r}, \bar{\Omega}', E' \right)}$$

$$\to \frac{\displaystyle\int_{g'}^{g'-1} dE' \left[\int_{g}^{g-1} dE \Sigma_s \left(\vec{r}, \bar{\Omega}' \to \Omega, E' \to E \right) \right] f \left(\vec{r}, E' \right)}{\displaystyle\int_{g'}^{g'-1} dE' f \left(\vec{r}, E' \right)} \equiv \Sigma_{s, g' \to g} \left(\vec{r}, \bar{\Omega}' \to \Omega \right).$$

(2.27)

We apply the definitions (Eqs (2.22) and (2.25)) and the approximations (Eqs (2.26) and (2.27)) to Eq. (2.24):

$$\bar{\Omega} \cdot \bar{\nabla} \psi_g \left(\vec{r}, \bar{\Omega} \right) + \Sigma_{tg} \left(\vec{r} \right) \psi_g \left(\vec{r}, \bar{\Omega} \right) =$$
$$Q_g \left(\vec{r}, \bar{\Omega} \right) + \int_{4\pi} d\Omega' \Sigma_{s, g' \to g} \left(\vec{r}, \bar{\Omega}' \to \Omega \right) \psi_{g'} \left(\vec{r}, \bar{\Omega}' \right),$$

(2.28)

where we have defined a group fixed plus in-scattering source:

$$Q_g \left(\vec{r}, \bar{\Omega} \right) = S_g \left(\vec{r}, \bar{\Omega} \right) + \sum_{\substack{g'=1 \\ g' \neq g}}^{G} \int_{4\pi} d\Omega' \Sigma_{s, g' \to g} \left(\vec{r}, \bar{\Omega}' \to \Omega \right) \psi_{g'} \left(\vec{r}, \bar{\Omega}' \right).$$

(2.29)

The multi-group equations are exact if the angular flux is separable and the energy spectrum is known (Eq. (2.30)) or if the cross sections are piecewise constant (Eq. (2.31)).

$$\psi\left(\bar{r},\bar{\Omega},E\right) = y\left(\bar{r},\bar{\Omega}\right)f\left(\bar{r},E\right),\qquad(2.30)$$

or

$$\Sigma_t\left(\bar{r},E\right) = C_1\left(\bar{r}\right) \text{ for } E_g \leq E \leq E_{g-1}, \text{ and}$$
$$\Sigma_s\left(\bar{r},E' \to E,\bar{\Omega}' \to \Omega\right) = C_2\left(\bar{r},\bar{\Omega}' \to \Omega\right) \text{ for } E_{g'} \leq E \leq E_{g'-1}.\qquad(2.31)$$

The multi-group equations are a coupled set of one-group equations each with the form given in Eq (2.33):

$$\bar{\Omega}\bullet\bar{\nabla}\,\psi\left(\bar{r},\bar{\Omega}\right) + \Sigma_t\left(\bar{r}\right)\psi\left(\bar{r},\bar{\Omega}\right) = Q_{ext}\left(\bar{r},\bar{\Omega}\right) + \int_{4\pi} d\Omega'\Sigma_s\left(\bar{r},\bar{\Omega}' \to \Omega\right)\psi\left(\bar{r},\bar{\Omega}'\right)\quad(2.32)$$

Solving multi-group time-dependent problems involves solving many equations in the form of Eq. (2.32). Solving an eigenvalue problem, with energy discretized by the multi-group method also requires solving many equations of the same form. For this reason we focus our research on finding solutions to equations in this form.

F. Discretization in Angle

It is convenient to expand the differential scattering cross sections in the orthogonal Legendre polynomials:[4]

$$\Sigma_s\left(\bar{r},\bar{\Omega}'\to\bar{\Omega}\right)=\frac{\Sigma_s\left(\bar{r},\mu_0\right)}{2\pi}=\sum_{l=0}^{\infty}\frac{(2l+1)}{4\pi}\Sigma_{sl}\left(\bar{r}\right)P_l\left(\mu_0\right) \qquad (2.33)$$

where we make the usual assumption that the scattering probability depends only on the

scattering angle, whose cosine is $\bar{\Omega}'\cdot\bar{\Omega}$:

$$\bar{\Omega}'\cdot\bar{\Omega}=\mu_0=\cos\text{ine of the scattering angle.} \qquad (2.34)$$

We can make this conclusion (that the scattering reaction depends on the angle

between the initial direction of travel and the final direction of travel) since we assumed

that the material has isotropic properties.

We have chosen to restrict the class of problems that we address in this work to

simplify our study, because even with restrictions the problem space is very rich. In our

case we will analyze problems with isotropic scattering and sources; therefore we

require only the zeroth moment in the scattering expansion:

$$Q\left(\bar{r},\bar{\Omega}\right)=\frac{1}{4\pi}\left[Q_{ext}\left(\bar{r}\right)+\int_{4\pi}d\Omega'\,\psi\left(\bar{r},\bar{\Omega}'\right)(1)\Sigma_{s0}\left(\bar{r}\right)P_0\left(\mu_0\right)^1\right] \qquad (2.35)$$

$$=\frac{1}{4\pi}\left[Q_{ext}\left(\bar{r}\right)+\Sigma_s\left(\bar{r}\right)\phi\left(\bar{r}\right)\right]. \qquad (2.36)$$

We use the definition of scalar flux to obtain Eq. (2.36); we then replace the right hand side of Eq. (2.32) to obtain the time independent one-group transport equation with isotropic sources:

$$\bar{\Omega} \cdot \bar{\nabla} \psi\left(\bar{r},\bar{\Omega}\right) + \Sigma_{t}\left(\bar{r}\right)\psi\left(\bar{r},\bar{\Omega}\right) = \frac{1}{4\pi}\left[Q_{ext}\left(\bar{r}\right) + \Sigma_{s}\phi(\bar{r})\right]. \tag{2.37}$$

F.1. Discrete Ordinate Method

One approach to discretizing the angular variable is to find the solution of the transport equation in specific angular directions. The discrete-ordinates method (commonly called S_N) does this and replaces angular integrals with quadrature sums:

$$\int_{4\pi} d\Omega f\left(\bar{\Omega}\right) \xrightarrow[\text{discrete-ordinates}]{} \sum_{m=1}^{M} w_m f\left(\bar{\Omega}_m\right), \tag{2.38}$$

where w_{m} and $\bar{\Omega}_{\mathrm{m}}$ constitute the mth weight and m^{th} direction respectively of the "quadrature set." Thus, the discrete-ordinates approximation for the "angular moments" (which appear in the scattering and fission terms) is:

$$\phi_{k,n}\left(\bar{r}\right) \xrightarrow[S_N]{} \sum_{\tilde{m}=1}^{M} w_{\tilde{m}} Y_{k,n}^{*}\left(\bar{\Omega}_{\tilde{m}}\right)\psi\left(\bar{r},\bar{\Omega}_{\tilde{m}}\right), \tag{2.39}$$

where Y_{kn}^{*} is the complex conjugate of the normalized spherical harmonics functions

Y_{kn}.[4] With the discrete-ordinates method, we need to find the angular flux only at M

different angles $\{\bar{\Omega}_m\}$. We define $\psi_m \equiv \psi(\bar{\Omega}_m)$ and rewrite Eq. (2.37) with the

expansion of the differential scattering cross section in the form of one-group discrete-

ordinates equations:

$$\bar{\Omega}_m \cdot \bar{\nabla} \psi_m(\bar{r}) + \Sigma_t(\bar{r}) \psi_m(\bar{r}) =$$
$$\frac{1}{4\pi} \left[Q_{ext}(\bar{r}) + \sum_{k=0}^{K} (2k+1) \Sigma_{s,k}(\bar{r}) \sum_{n=-k}^{k} \phi_{k,n}(\bar{r}) Y_{k,n}(\bar{\Omega}_m) \right] \quad m = 1,\ldots,M. \tag{2.40}$$

Thus, by replacing the integral over the direction variable with a quadrature sum, we

can reduce the steady state one-group transport equation to a set of coupled first order

differential equations in which the unknowns ψ_m depend only on position. The

following well known production codes utilize the discrete-ordinates method for neutral

particle transport, TORT[14] and PARTISN.[15] In problems with isotropic scattering

$(K=0)$ one only needs the 0th angular moment, therefore Eq. (2.40) becomes:

$$\bar{\Omega}_m \cdot \bar{\nabla} \psi_m(\bar{r}) + \Sigma_t(\bar{r}) \psi_m(\bar{r}) = \frac{1}{4\pi} \left[Q_{ext}(\bar{r}) + \Sigma_s(\bar{r}) \phi(\bar{r}) \right], \quad m = 1,\ldots,M , \tag{2.41}$$

where

$$\phi(\bar{r}) \equiv \sum_{\tilde{m}=1}^{M} w_{\tilde{m}} \psi_{\tilde{m}} . \tag{2.42}$$

F.2. Other Methods

Another approach to angular discretization is to assume that $\psi(\bar{\Omega})$ is a linear combination of known basis functions:

$$\psi(\bar{r},\bar{\Omega}) \xrightarrow[\substack{function \\ expansion}]{} \sum_{m=1}^{M} \tilde{\psi}_m(\bar{r}) b_m(\bar{\Omega}) \tag{2.43}$$

The coefficients $(\tilde{\psi}_m)$ are unknown; the moments of the basis functions (b_m) are known. A standard way of finding the coefficients in a function expansion is the weighted-residual approach. This approach inserts the function expansion into the equation and defines the residual as the difference between the right- and left-hand sides of that equation. If the residual is zero for all values of $\bar{r}$ and $\bar{\Omega}$ then the expansion is perfect.

This ideal result almost never happens. However, it is possible to choose the expansion coefficients so that the residual is minimized in some sense. For example, we could force M different weighted integrals of the residual be zero. This is called the weighted-residual approach. Insert Eq. (2.43) into Eq.(2.37) and expand the scattering source:

$$\left[\bar{\Omega}\bullet\bar{\nabla}+\Sigma_t\left(\bar{r}\right)\right]\sum_{m=1}^{M}\tilde{\psi}_m\left(\bar{r}\right)b_m\left(\bar{\Omega}\right)=$$

$$\frac{1}{4\pi}\left[Q_{ext}\left(\bar{r}\right)+\sum_{k=0}^{K}\left(2k+1\right)\Sigma_{s,k}\left(\bar{r}\right)\sum_{n=-k}^{k}\phi_{k,n}\left(\bar{r}\right)Y_{k,n}\left(\bar{\Omega}_m\right)\right],$$

(2.44)

where

$$\phi_{k,n}\left(\bar{r}\right)\equiv\sum_{\tilde{m}=1}^{M}\tilde{\psi}_{\tilde{m}}\left(\bar{r}\right)\int_{4\pi}d\Omega Y_{k,n}^{*}\left(\bar{\Omega}\right)b_m\left(\bar{\Omega}\right)$$

(2.45)

Then for some set of M weight functions $\left(w_m\right)$, we require:

$$\int_{4\pi}d\Omega w_m\left(\bar{\Omega}\right)\left[\bar{\Omega}\bullet\bar{\nabla}+\Sigma_t\left(\bar{r}\right)\right]\sum_{m=1}^{M}\tilde{\psi}_m\left(\bar{r}\right)b_m\left(\bar{\Omega}\right)=$$

$$\frac{1}{4\pi}\int_{4\pi}d\Omega w_m\left(\bar{\Omega}\right)\left[Q_{ext}\left(\bar{r}\right)+\sum_{k=0}^{K}\left(2k+1\right)\Sigma_{s,k}\left(\bar{r}\right)\sum_{n=-k}^{k}\phi_{k,n}\left(\bar{r}\right)Y_{k,n}\left(\bar{\Omega}_m\right)\right],\ m=1\ldots M.$$

(2.46)

This yields M equations for the M expansion coefficients $\left(\tilde{\psi}_m\right)$. If the weight and

basis functions are spherical harmonic functions through order N then this is called the

"spherical harmonics" or P_N method. If the weight and basis functions are nonzero only

over small local portions of the direction domain, this is called a finite-element method

(FEM) in angle. If the weight and basis functions span the same function space, the

weighting is called Galerkin weighting.

G. Spatial Discretization

We begin with the discrete-ordinates equations (Eq. (2.41)) in two-dimensional

Cartesian coordinates:

$$\left[\mu_m \frac{\partial}{\partial x} + \eta_m \frac{\partial}{\partial y} + \Sigma_t(x,y)\right]\psi_m(x,y) = \frac{1}{4\pi}\left[Q_{ext}(x,y) + \Sigma_s(x,y)\phi(x,y)\right],$$

$$m = 1,\ldots,M, \tag{2.47}$$

where

$$\mu_m = \bar{\Omega}_m \bullet \bar{e}_x \text{ and } \eta_m = \bar{\Omega}_m \bullet \bar{e}_y. \tag{2.48}$$

We examine an arbitrary cell from a rectangular grid and direction, $\bar{\Omega}_m$ as shown in

Figure 4.
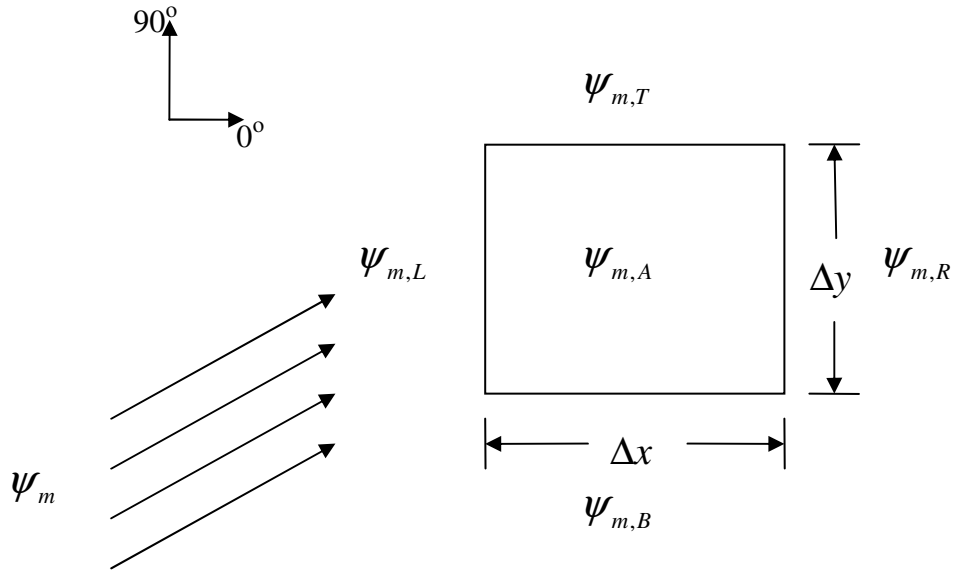
Figure 4   A rectangular cell with an angular flux entering through the left (L) and bottom (B) edges and exiting through the top (T) and right (R) edges.

We suppress the direction subscript, m and define the fluxes averaged over the cell edges and area respectively as:

$$\psi_R = \frac{1}{\Delta y} \int_0^{\Delta y} dy\, \psi(\Delta x, y)\,;$$

(2.49)

$$\psi_T = \frac{1}{\Delta x} \int_0^{\Delta x} dx\, \psi(x, \Delta y)\,;$$

(2.50)

$$\psi_A = \frac{1}{\Delta x \Delta y} \int_0^{\Delta y} dy \int_0^{\Delta x} dx\, \psi(x, y)\,;$$

(2.51)

$$q_A = \frac{1}{\Delta x \Delta y} \frac{1}{4\pi} \int\limits_0^{\Delta y} dy \int\limits_0^{\Delta x} dx \left[Q_{ext}(x,y) + \Sigma_s(x,y)\phi(x,y) \right]. \qquad (2.52)$$

ψ_L and ψ_B are defined similarly. We now integrate Eq. (2.47) over the cell area and

divide by $\Delta x \Delta y$ in order to obtain the balance equation for the cell:

$$\psi_A = \frac{q_A}{\Sigma_t} - \frac{(\psi_R - \psi_L)}{\tau_x} - \frac{(\psi_T - \psi_B)}{\tau_y}, \qquad (2.53)$$

where

$$\tau_x = \frac{\Sigma_t \Delta x}{\mu} \text{ and } \tau_y = \frac{\Sigma_t \Delta y}{\eta}. \qquad (2.54)$$

Equation (2.53) contains no spatial approximation and therefore is exact.[4] For this

research we have chosen to use the Step Characteristic method, which assumes the

scattering and fixed sources are constant in each cell. The total macroscopic cross

section is constant throughout the cell. Incident and exiting angular fluxes are averaged

over their respective cell edges.

The Step Characteristic (SC) method was first developed by Lathrop.[16] Although we

derive our SC method in rectangular cells, the original derivation of the method does not

make assumptions about the shape of the cell.

The exit flux for the cell in Figure 4 can be expressed in terms of a suitable linear combination of the incident flux and the average source term, (q_A). For example, in Fig. 4 the direction of interest is such that exiting angular flux through the top surface depends only on the incident flux through the left surface and q_A:

$$\psi_T = \psi_L M_0(\tau_x) + \frac{q_A}{\Sigma_t}\left[1 - M_0(\tau_x)\right], \qquad (2.55)$$

where we use exponential moment function defined by Walters:[17]

$$M_0(\tau_x) = \frac{\left(1 - e^{-\tau_x}\right)}{\tau_x}. \qquad (2.56)$$

The SC method is monotonic, positive and simple, but somewhat diffusive. On square cells in the Cartesian coordinate system it has the added disadvantage of characteristic anomalies at all $\frac{n\pi}{4}$ directions. These anomalies effectively cause inaccuracies in angular flux and all angular moments of angular flux. Despite these flaws, it is well suited for the research we present in this dissertation. We present a more detailed derivation of the SC formulas in Appendix A.

H. Solution Methods

We use source iteration (iteration on the scattering source) in this research for solving simultaneous equations. Calculations are made using "iterative sweeps" in the direction of particle flow. Each iteration consist of four sweeps through a rectangular grid mesh:

$$\mu > 0, \quad \eta > 0 \qquad \text{left to right; bottom to top.} \qquad (1)$$
$$\mu < 0, \quad \eta > 0 \qquad \text{right to left; bottom to top.} \qquad (2)$$
$$\mu < 0, \quad \eta < 0 \qquad \text{right to left; top to bottom.} \qquad (3)$$
$$\mu > 0, \quad \eta < 0 \qquad \text{left to right; top to bottom.} \qquad (4)$$

The source in each cell is updated using the discrete-ordinates approximation Eq. (2.42):

$$q_A = \frac{1}{4\pi} \left[Q + \Sigma_s \phi_A \right]. \qquad (2.57)$$

I. Summary

Deterministic solutions of the particle transport equation are difficult. However, they are made more manageable when they are reduced to coupled sets of one-group fixed-source steady-state equations. In this section we reviewed some of the ways that the transport equation's variables can be discretized:

- Finite-differencing the derivative in time;

- The multi-group approximation for energy;

- The discrete-ordinates method in angle;

- 2-D Cartesian geometry step characteristic for position.

We also outlined the source-iteration procedure for solving the discrete equations.

III. QUADRATURE RULES

The classical quadrature rule is based on the following equation:

$$\int_a^b w(x) f(x) dx = \sum_{i=1}^N w_i f(x_i) + E.$$

$$(3.1)$$

The set of $\{x_i\}$ are the quadrature nodes or abscissae, $w(x)$ is the weight function and $\{w_i\}$ are the quadrature weights. N is the number of points in the quadrature set and E is the error. A quadrature formula is said to have n^{th}-order precision if it exactly integrates all polynomials of degree n or less. The values of $\{w_i\}$ and $\{x_i\}$ depend on the interval of integration $[a,b]$ and on the weight function. If a set $\{x_i\}$ does not include the endpoints a and b the rule is said to be an open rule. An open rule is useful when evaluating integrals that exhibit endpoint singularities. A closed rule includes the endpoints of the range.

A. Newton-Cotes Rules

Newton-Cotes rules are formulas for a constant weight function and a finite interval of integration.[18] The two "primitive rules" are the mid-point rule, shown in Eq. (3.2), and the trapezoidal rule, shown in Eq. (3.3):

$$\int_a^b f(x)\,dx \simeq h\sum_{i=1}^N f(p_i) = M_N(f); \qquad (3.2)$$

$$\int_a^b f(x)\,dx \simeq \frac{h}{2}\left[f(a) + \left\{ 2\sum_{i=1}^{N-1} f(q_i) \right\} + f(b) \right] = T_N(f) \qquad (3.3)$$

The interval of integration $[a,b]$ is divided into N segments of length $h = \dfrac{b-a}{N}$. The mid-point rule is an open rule, where the quadrature points p_i are:

$$p_i = \left\{ a + \frac{(2i-1)}{2}h \right\}, \quad i=1,\ldots,N; \qquad (3.4)$$

the trapezoidal is a closed rule, where the quadrature set includes the end points a and b and points q_i, which are:

$$q_i = \{ a + ih \}, \quad i=1,\ldots,N-1. \qquad (3.5)$$

There derivations are simple and they are likely to be the first rules introduced in any common math text.

Another simple, higher order and commonly used rule is Simpson's rule. The beauty of Simpson's rule, and the reason it is so widely used, is that it is derived to integrate

exactly a quadratic polynomial, but the resulting formula integrates a cubic

polynomial:[19]

$$\int_a^b f(x)\,dx \simeq \frac{h}{3}\left[f(a) + 4\sum_{\substack{i=1 \\ i\,odd}}^{2N-1} f(a+ih) + 2\sum_{\substack{i=2 \\ i\,even}}^{2N-2} f(a+ih) + f(b) \right] = S_{2N}(f). \quad (3.6)$$

Although we do not examine Simpson's rule directly, we will introduce another rule that

has some similarities to Simpson's rule in the azimuthal angle space.

B. Level Symmetric Rule

Level-symmetric quadrature rules are widely used when solving the Boltzmann

transport equation.[20] The ordinates are arranged on the unit octant bounded by axes in

the direction cosines $(\mu,\ \eta,\ \text{and}\ \zeta)$. The set of positive values on each axis are the

same:

$$\mu_n = \eta_n = \zeta_n \quad n = 1, 2, \ldots, \frac{N}{2} \qquad (3.7)$$

The set of ordinate directions is invariant to 90° rotations about any axis. A widely

used level-symmetric set of order N has only one degree of freedom.[4] The weights are

determined using a geometric association described in Ref. 3. One significant drawback of the level-symmetric quadrature rule is negative weights for $N > 20$.

C. Gaussian Rules

More advanced rules (e.g. the theory of Gaussian quadrature) choose the abscissae $\{x_i\}$ in addition to the weights $\{w_i\}$ to maximize the order of the polynomials that they integrate. Finding the $\{x_i\}$ requires the solution of non-linear equations, whose solutions are based on the zeros of an associated set of orthogonal polynomials. An *N*-point Gaussian quadrature rule yields an exact result for polynomials of degree $2N - 1$. There are Gaussian quadrature rules associated with Legendre polynomials, Jacobi polynomials and Chebyshev polynomials of the first kind.

The Gaussian based rules that we examine in this work are based on the Chebyshev polynomials of the first kind and the polynomials developed by I. K. Abu-Shumays. We do not attempt any refinements in the level-symmetric quadrature sets.

Abu-Shumays' work takes advantage of the inherent symmetries in two dimensions in order to develop accurate angular quadrature abscissae and weights "especially suited for the net and/or partial currents and all the net and/or partial moments of the neutron flux."[21] His work details the use of Chebyshev-Gauss rules to derive product quadrature sets to solve integrals in the form of Eq. (3.8):

$$\int_{\bar{\Omega}} f\left(\Omega_x, \Omega_y\right) d\bar{\Omega} = \int_0^{2\pi} d\gamma \int_0^{\pi} \sin\theta f\left(\sin\theta\cos\gamma, \sin\theta\sin\gamma\right)$$

$$\cong \sum_{i=1}^{4\tau} \sum_{j=1}^{N} w_i^I w_j^K f\left(\sin\theta_j \cos\gamma_i, \sin\theta_j \sin\gamma_i\right).$$

(3.8)

Abu-Shumays divides his integral into a product quadrature set between the polar (θ) and azimuthal (γ) directions. Since two dimensional problems are relatively smooth in the polar directions, the real interest and difficulties lie in the azimuthal directions. The Abu-Shumays quadrature sets enumerated in his paper will accurately integrate higher order polynomials in the form of Eq.(3.9).

$$\int_0^{\pi/2} \left(\cos^l \gamma \sin^m \gamma\right) d\gamma$$

(3.9)

D. Disadvantages of "Static" Quadrature Rules

The Gaussian quadrature and other such advanced rules can have high accuracy compared to Newton-Cotes rules, but at a potentially high cost. It is a common practice when comparing quadrature rules to take an increasing size (number of abscissae) and show their accuracy when solving a particular integral. If one were to use a generalized Simpson's rule each time the size of the quadrature set doubled the Simpson rule uses the points from the previous set (i.e. 2, 4, 8, 16 …). Therefore the number of function evaluations are $2+2+4+8\cdots$. A comparable Gaussian function evaluation does not use

the same points from the previous set. The Simpson sets yields answers at half the cost of the Gaussian. Although it may be less accurate, a progressive rule like Simpson's may be more useful with its lower cost.

All quadrature rules have difficulty when they are used to evaluate a region where a sharp "spike" or discontinuity may be present (a "peaky" function). Although convergence may appear to occur without any complications, the unseen spike in an otherwise smooth function (or data) can create different answers as one changes the size of the quadrature set. If one knows how a rule works, it is a relatively simple task to invent a problem that defeats it.

Oscillatory problems can pose a huge difficulty for most quadrature rules as well. This is especially true when the number of oscillations is greater than the density of the abscissae in the quadrature set. These problems arise quite frequently in reactor physics and source shielding problems. They are the main cause of the so-called *ray effects* that were defined in a previous section. Another approach to solving these problems is to move the oscillatory part of the problem into the weight function of Eq. (3.1). It is possible to generate a Gaussian formula with the weight functions $\cos(\omega x)$ and $\sin(\omega x)$. However, this approach is extremely expensive since it requires different rules for different combinations of intervals of integration, oscillatory rates (ω) and types of oscillation (e.g. trigonometric or Bessel). One of the earliest attempts at such an approach was made by Filon.[22]

Singularities are also a major hurdle to over come when finding a rule to solve an integral. Most attempts of solutions to these problems involve the careful selection of a

quadrature set to avoid the placement of a point near or on the singularity. Here, like in the oscillatory problems, it is possible to come up with special weighted Gaussian rules to solve unique problems, but these are also very expensive and require prior knowledge of the locations of the singularities. In real world problems, for example reactor physics and shielding, the analyst can not always be certain where a singularity will occur.

A more practical approach is to begin with a Newton-Cote rule and refine the range of integration where more points are needed to accurately interpolate the function. A higher accuracy can be obtained through subdividing of the range around the singularities.

E. Adaptive Quadrature Rules

Rules are said to be adaptive if they automatically change the size of the quadrature set through refinement or coarsening in difficult regions within the range of integration. The popularity of automatic integrators is directly related to the advent of the computer age.

Adaptive discrete-ordinate rules are generally problem specific locally refined approaches (locally refine a quadrature set to provide a very high number of angles in a directional cone). Longoni and Haghighat developed a technique they call Ordinate Splitting. The idea is to select a direction of flight of the particle and split it into a certain number of directions of equal weights, while conserving the original weight.[23] In another technique they call "regional angular refinement" or RAR, Longoni and Haghighat begin with a P_N-T_N quadrature set of arbitrary order on one octant of a unit

sphere. They use the Legendre polynomials in the polar direction and Chebyshev polynomials of first kind in the azimuthal direction to generate extra quadrature points in specific regions (directions) inside the octant.[24] Brown and Chang use a simple quadrature rule to subdivide the cone using triangular tessellations in 3D and rectangular tessellations in 2D.[25]

The simplest adaptive rule makes use of a progressive rule by starting with a small number of points and successively dividing the range until the desired accuracy is achieved. The simple idea here is to increase the number of quadrature points in a trouble region and eventually have a dense enough concentration of quadrature points to evaluate it properly. Quadpack by Piessens, Doncker-Kapenga, Überhuber and Kahanr is one of the more well known packages for solving difficult mathematical problems.[26] In this package the authors subdivide the intervals of integration based on error calculation over subintervals, applying a finer quadrature set to each sub-interval. The quadrature rules most utilized for this approach are the Gauss-Kronrod rules. They are employed by many software packages (e.g. Quadpack and Mathemattica™). These formulae rely on the error estimation at the so called "Kronrod points," which are based on the zeros of Legendre polynomials and Stieltjes polynomials. The major advantage of this method is to allow the reuse of previously evaluated abscissae, that is to say it is progressive. One of the major drawbacks of the Gaussian rules is that they are not progressive. Kronrod showed that by adding $n+1$ abscissae to the Gaussian rule it was possible to generate a quadrature rule which would be progressive and integrate exactly polynomials of degree $3n+1$ for n even $3n+2$ for n odd.[27] Quadpack and many other

mathematical packages (mainly written in FORTRAN) are available online at http://gams.nist.gov/.

We postulate that an adaptive method would be extremely helpful in our goal to mitigate ray effects and other discretization errors in the discrete-ordinates approximation. Using an adaptive method like the one described above could be very expensive when solving the transport equation. Our approach is start with a Newton-Cotes or Gaussian rule, then efficiently add quadrature points at specific trouble spots (at sharp peaks or around singularities) in the angular flux function. We describe our approach in detail in Section 4.

F. Summary

The "primitive" Newton-Cotes rules are simple yet useful as starting quadrature sets for adaptive algorithms. The level-symmetric rule is commonly used in today's transport calculations; however it is limited to order S_{20} and it is not adaptable. The Gaussian rules are more advanced but can be expensive to implement. Adaptive rules are becoming very popular and could be very useful to mitigate ray effects and other angular discretization errors in discrete-ordinates approximations.

IV. THE ADAPTIVE STRATEGY

A. The Argument

Our adaptive algorithm by necessity uses more computer processor (cpu) time per unknown. This investment is made in order to compare interpolative values with computed transport values. However, this hindrance can be mitigated by the reduced number of unknowns to achieve a given accuracy. It can be further mitigated in time-dependent problems, where the cpu time necessary for our adaptive logic can be amortized over several time steps. In other words, it may not be necessary to adapt on every time step in a time-dependent problem (or even every iteration in a steady-state problem). In addition, an adaptive algorithm produces a given accuracy with significantly fewer unknowns in general, resulting in significant memory savings. This savings can be very important in particle-transport problems. One could also argue that it may be well worth additional expense to provide the user confidence that the solution is accurate to within the tolerance specified.

B. The Adaptive Algorithm

The two-dimensional problems we analyze in this work have relatively smooth solutions in the polar direction and therefore may be integrated with relatively few Gaussians polar-quadrature points. Thus, there exists a "product quadrature set" that can accurately perform the needed angular integrals. By "product" quadrature we mean the

combination of two one-dimensional quadrature sets (one in the polar direction and one in the azimuthal). We write our product quadrature approximation in the following manner:

$$\int_{4\pi} \psi\left(\bar{r},\bar{\Omega}\right)d\Omega = \int_{0}^{\pi}\int_{0}^{2\pi} \psi\left(\bar{r},\gamma,\theta\right)d\gamma \sin\theta d\theta$$
$$\xrightarrow[\substack{product \\ quadrature}]{} \sum_{m=1}^{M_p} w_{p,m} \sum_{n=1}^{M_{a,m}} w_{a,n}^{m} \psi\left(\bar{r},\gamma_n^m,\theta_m\right).$$

(4.1)

Product quadratures are not a new idea for transport calculations. For example, Abu-Shumays derived Gaussian class quadrature sets that he presented as "product formulas."[28] In Eq (4.1) θ and γ are the polar and azimuthal directions, respectively. Notice that the azimuthal direction has the m index to specify that each polar level may have its own set of azimuthal angles independent of other levels. Typical quadrature sets will have a varying number of azimuthal angles on each level with more toward the equator and fewer near the pole of the polar dimension (e.g. level symmetric quadrature sets). For simplicity, in our current implementation we require all polar levels to have the same azimuthal quadrature set before adaptive refinement.

We divide the spatial domain into regions and divide each region into cells. All cells within the spatial region have the same quadrature set. We apply our adaptive logic to the exiting angular flux along each region boundary. We determine the interpolative angular flux values (or extrapolative values near the ends of the "open" intervals). We compare these values against the actual exiting flux that is calculated by "sweeping" the

region at the test direction. If the relative difference between these values does not meet a user provided tolerance then the test point is added to the quadrature list.

At least one iterative sweep of the problem must be completed before any refining of a quadrature set can commence. If the problem has some highly scattering regions in it, then it may be preferable to perform many iterative sweeps before performing any adaptive process. This allows the problem to step towards convergence and achieve more accurate values for exiting flux, thus providing a more accurate interpolation. The user determines how often to perform the refinement process. However, in the purely absorbing case, there is no scattering source to converge; therefore, in purely absorbing problems we adapt after every iterative sweep.

If a refinement test is to be made on the next iterative sweep the values of exiting angular flux on region boundaries are stored during the current iterative sweep. The refinement sweep (a modified iterative sweep) is conducted on a region by region basis (one polar level at a time). Figure 5 illustrates a linear test adaptive method.
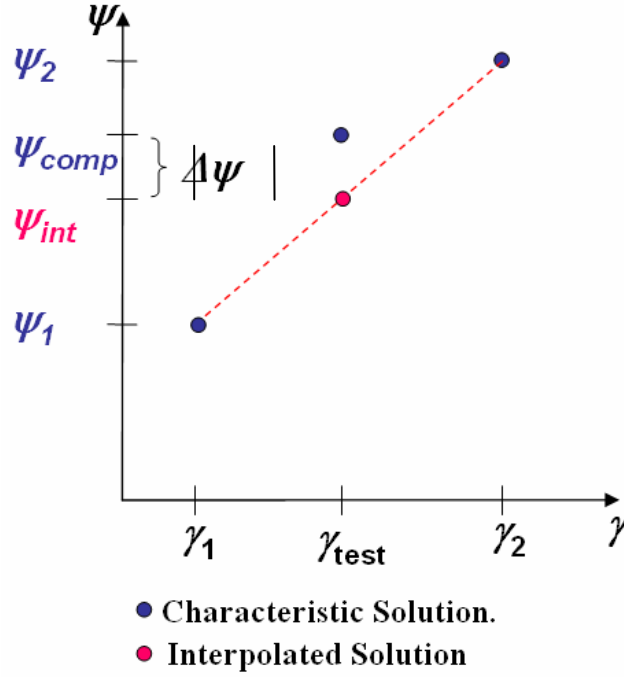
Figure 5   A linear-interpolation adaptive method.

Angular fluxes ψ_1 and ψ_2 at quadrature points γ_1 and γ_2 are the results stored from the previous iterative step. In the testing phase of the algorithm, we evaluate a test angular flux $\left(\psi_{comp}\right)$ at the midpoint $\left(\gamma_{\text{test}}\right)$ between γ_1 and γ_2. We evaluate the interpolated angular flux $\left(\psi_{int}\right)$ at the same test angle using an interpolative method chosen by the user. We compare the absolute value of the difference between the two values $\left(\left|\Delta\psi\right|\right)$ against the tolerance criterion $\left(TC\right)$:

$$TC = \varepsilon_{re}\left[\left|\psi_{comp}\right| + \varepsilon_{th}\frac{\sum\limits_{m=1}^{N}\psi_m}{N}\right].$$

(4.2)

The relative error $\left(\varepsilon_{re}\right)$ and threshold tolerance $\left(\varepsilon_{th}\right)$ are user specified. The threshold tolerance, multiplied by an average angular flux evaluated in the cell, is a limiter to the adaptive process. It helps prevent "over-adapting." There may be some ranges of flux that are extremely small compared with the overall angular flux function. This added tolerance helps to ensure that the algorithm does not continue to adapt to resolve ever smaller and possibly insignificant angular flux. However, although a value may seem insignificant at one spatial point, it may be significant elsewhere. If there is not an appropriate refinement taking place, the user can use a larger initial starting quadrature set or set the threshold tolerance, ε_{th}, to a very small value. As $\varepsilon_{th} \rightarrow 0$ the TC becomes simply a relative-error test.

After all midpoints in a region list have been tested (on every polar level within a quadrant), the adaptive logic adds the test angles that failed the tolerance test ($\left|\Delta\psi\right| > TC$) to the region's quadrature set. If the test angle passes the test ($\left|\Delta\psi\right| < TC$), the adaptive logic accepts the interpolated value of angular flux as the correct angular flux, therefore rejecting the test point. This procedure may cause neighboring regions to have different quadrature sets, which sometimes requires the use of interpolated values from one region as incident angular fluxes on adjacent regions. Once all testing in a region is complete, the program calculates a new region scalar flux using a normal iterative sweep. We update the scattering source after all regions have been refined and then swept with their new quadrature sets.

C. Conservation

Since each region locally refines the initial quadrature list to its own needs, the quadrature sets of neighboring regions will likely be different. In Figure 6 we have illustrated this difference. To conserve particle flow, we require the exiting partial current through each region's surface to be identical to the incident partial current of the adjacent region's surface. However, given different quadrature sets, this will not happen in general unless we take steps to enforce it.
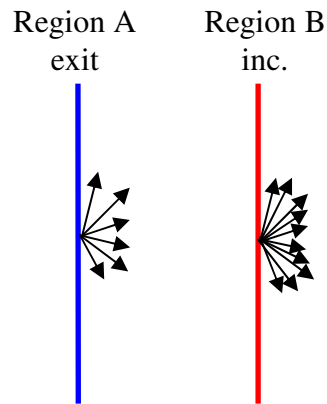

Figure 6   Example in which the quadrature set of region A has fewer points than the quadrature set of region B.

The angular current density is a vector quantity defined by:

$$\vec{j}\left(\vec{r}, E, \vec{\Omega}, t\right) = \vec{\Omega}\,\psi\left(\vec{r}, E, \vec{\Omega}, t\right). \tag{4.3}$$

If $\bar{e}_n$ is the unit normal vector to the area d^2r then we define the discrete partial

current:

$\bar{e}_n \cdot \bar{j}(\bar{r}, E, \bar{\Omega}, t) d^2r \, d\Omega \, dE \, dt \equiv$ is the number of particles crossing the area

$$d^2r \text{ about } \bar{r}, \text{ with energies in } dE \text{ about } E \text{ and} \quad (4.4)$$

directions $d\Omega$ about $\bar{\Omega}$, in time dt.

If it is a positive quantity then flow is in the direction of $+\bar{e}_n$ and if it is negative then

flow is in the direction of $-\bar{e}_n$.

Partial current density is a non-negative scalar quantity defined as the rate per unit

area at which particles cross an area d^2r from one side to the other. Mathematically,

partial current toward the $+\bar{e}_n$ side is defined:

$$J_e^+(\bar{r}, E, t) = \int_0^{2\pi} d\gamma \int_{\bar{\Omega}:\bar{e}_n \cdot \bar{\Omega} > 0} d\Omega \left(\bar{e}_n \cdot \bar{\Omega} \right) \psi(\bar{r}, E, \bar{\Omega}, t) \quad (4.5)$$

or

$$J_e^+(\bar{r}, E, t) = \int_0^{2\pi} d\gamma \int_{\mu>0} d\mu(\mu) \psi(\bar{r}, E, \bar{\Omega}, t), \quad (4.6)$$

where μ is the direction cosine $\left(\bar{e}_n \cdot \bar{\Omega}\right)$. The partial current density in the $-\bar{e}_n$ direction is defined:

$$J_e^-\left(\bar{r}, E, t\right) = \int\limits_0^{2\pi} d\gamma \int\limits_{\mu<0} d\mu |\mu| \psi\left(\bar{r}, E, \bar{\Omega}, t\right) \tag{4.7}$$

After all refinements are complete and the convergence criteria have been achieved we perform one last sweep of the problem. We define a scaling factor (SF) as the ratio of the exiting partial current to the "old" incident partial current.

$$SF = \frac{\displaystyle\sum_{m=1}^{M_{exit}} w_m \mu_m \psi_m}{\displaystyle\sum_{n=1}^{N_{inc}} w_n \mu_n \psi_n^{old}} \tag{4.8}$$

As with all previous sweeps of the problem, we must acquire the incident angular flux (for "Region B") from the values of the exiting angular flux (of "Region A"). We refer to this incident angular flux as the "old" incident angular flux $\left(\psi_n^{old}\right)$. The "old" incident angular flux is either directly equal to an exiting angular flux (i.e. they have the same direction) or it is the interpolant of the exiting angular flux. Before a sweep of a region is commenced, all of the "old" incident angular fluxes are calculated and used to determine the SF. We use the SF to calculate a "new" incident angular flux:

$$\psi_n^{new} = (SF)\psi_n^{old}.$$ (4.9)

D. The Quadrature Rules for Our Adaptive Methods

There are many different algorithms for adaptive quadrature rules. J. R. Rice claims that there are as many as 10 million different adaptive algorithms of interest with significant differences from one another.[29] We concentrate our research on three types of quadrature rules and three similar adaptive algorithms.

D.1 Linear

In the first adaptive method we interpolate the exiting angular flux one point at a time with a mid-point rule (open). This method uses a linear interpolation in the azimuthal dimension:

$$f(\gamma) = A\gamma + B$$ (4.10)

We calculate a set of Chebyshev abscissae (Eq. (4.11)) for the initial population of all the quadrature sets:

$$\gamma_m = \frac{(2m-1)\pi}{4N} \quad \{m = 1, 2, \ldots, N\}.$$ (4.11)

where N is the number of abscissae per quadrant.

Since we employ a Cartesian grid system for our spatial discretization, discontinuities in the angular flux at a given spatial point can occur at the quadrant boundaries $\left(0, \dfrac{\pi}{2}, \pi, \dfrac{3\pi}{2}\right)$. This difficulty makes a closed quadrature rule on a quadrant basis hard to manage; therefore we begin with a mid-point rule on the range 0 to 2π. We divide the range into the usual four quadrants. Obviously this also divides the quadrature points into four sets.

An example $N = 3$ points per quadrant quadrature set is shown below. Note that this is the initial (before first refinement) quadrature set and that each region, polar level and quadrant starts with an identical number (N) of equally spaced abscissae per quadrant:

$$QS_M^3 \left(region,\ polar\ level,\ quadrant = 1\right) = \left\{\frac{\pi}{12}, \frac{3\pi}{12}, \frac{5\pi}{12}\right\} \tag{4.12}$$

The initial weights for the quadrature sets are the normal midpoint-rule weights (please refer to Eq. (3.2)):

$$w\left(QS_M^3\right)\left(region,\ polar\ level,\ quadrant = 1\right) = \left\{\frac{\pi}{6}, \frac{\pi}{6}, \frac{\pi}{6}\right\} \tag{4.13}$$

Since these are Chebyshev points, these quadrature sets exactly integrate the $2N^{th}$-order

Chebyshev polynomials on the global interval $[0, 2\pi]$. We discuss this observation in

more detail in section C. 3 (the third adaptive algorithm).

The midpoint angles between the existing abscissae of the quadrature sets are

examined in each test phase. Since the mid-point rule is open, we must also examine the

angles between the extremes of the quadrature set and the quadrant boundaries. We

extrapolate using the two values at either the beginning or end of the quadrature list (see

Figure 7). We choose the test angles for the extrapolated points such that they are a

sufficient distance away from the extreme values in the quadrature list. We do this in

order to approach singularities (if they exist) at the quadrant boundaries as quickly as

possible:

$$\gamma_{\text{test end point min}} = \frac{2\gamma_{\min} + \gamma_1}{3} \qquad (4.14)$$

$$\gamma_{\text{test end point max}} = \frac{2\gamma_N + \gamma_{\max}}{3} \qquad (4.15)$$

The minimum azimuthal value $(\gamma_{\min})$ is the lower extreme of the quadrant boundary

$\left([q-1]\frac{\pi}{2}\right)$ and the maximum azimuthal value $(\gamma_{\max})$ is the upper extreme of the

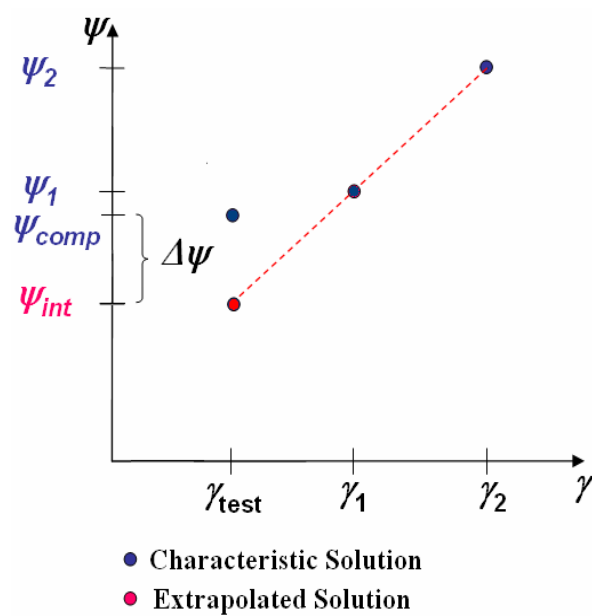quadrant boundary $\left(q\frac{\pi}{2}\right)$, where $q = 1, 2, 3, 4$.

Figure 7   Example of the extrapolative linear test.

When new abscissae are added to a quadrature set new weights are calculated for the neighboring points. Our guiding principle for calculating quadrature weights is that we maintain consistency with an underlying finite-element basis set. That is, we construct an interpolatory "basis function" for each quadrature point and integrate it to obtain the weight for that point. In the current setting, with linear interpolation, we integrate the linear "tent" functions associated with each abscissa (as shown in Figure 8 and Figure 9). This means that the mid-point rule for the whole range (0 to 2π) only holds in the unrefined quadrature set. Once the quadrature set has been refined the mid-point rule is no longer valid over the whole range.
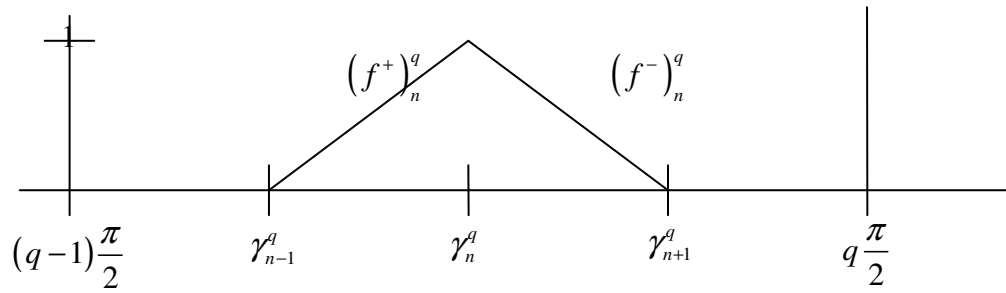
Figure 8   Linear weight functions in quadrant q.

The weight of γ_n^q is:

$$w_n^q = \int_{\gamma_{n-1}^q}^{\gamma_n^q} d\gamma \left(f^+\right)_n^q + \int_{\gamma_n^q}^{\gamma_{n+1}^q} d\gamma \left(f^-\right)_n^q \tag{4.16}$$

where $\left(f^+\right)$ is the positive sloping linear function and $\left(f^-\right)$ is the negative sloping

linear function. At the extreme values of the quadrant, it is necessary to integrate from

the extreme quadrature points of the neighboring quadrants as shown in Figure 9.
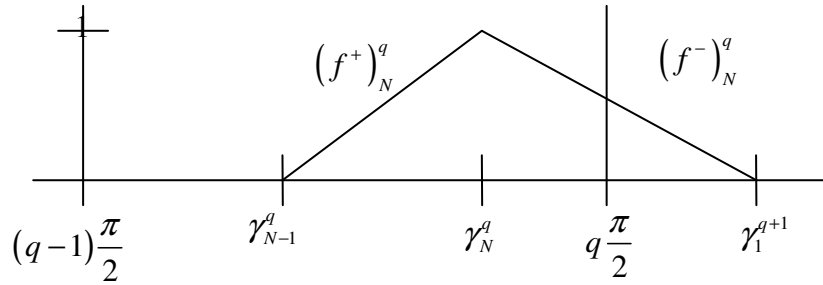
$$(q-1)\frac{\pi}{2} \qquad \gamma_{N-1}^{q} \qquad \gamma_{N}^{q} \qquad q\frac{\pi}{2} \qquad \gamma_{1}^{q+1}$$

Figure 9   Linear weight functions at the extreme of quadrant q.

D.2.   Linear in Sine and Cosine

The second adaptive algorithm employs basis functions that are linear in $\sin(\gamma)$ and $\cos(\gamma)$. It is similar to a 3-point Simpson rule. We refer to it by the acronym LSC:

$$f(\gamma) = A\cos(\gamma) + B\sin(\gamma) + C \equiv A\mu + B\eta + C \qquad (4.17)$$

In Figure 10 we choose three arbitrary angles (separated by $\Delta\gamma$) in a quadrant domain on the range of $[\gamma_a, \gamma_b]$. The three basis functions have a shape similar to quadratic functions in γ.
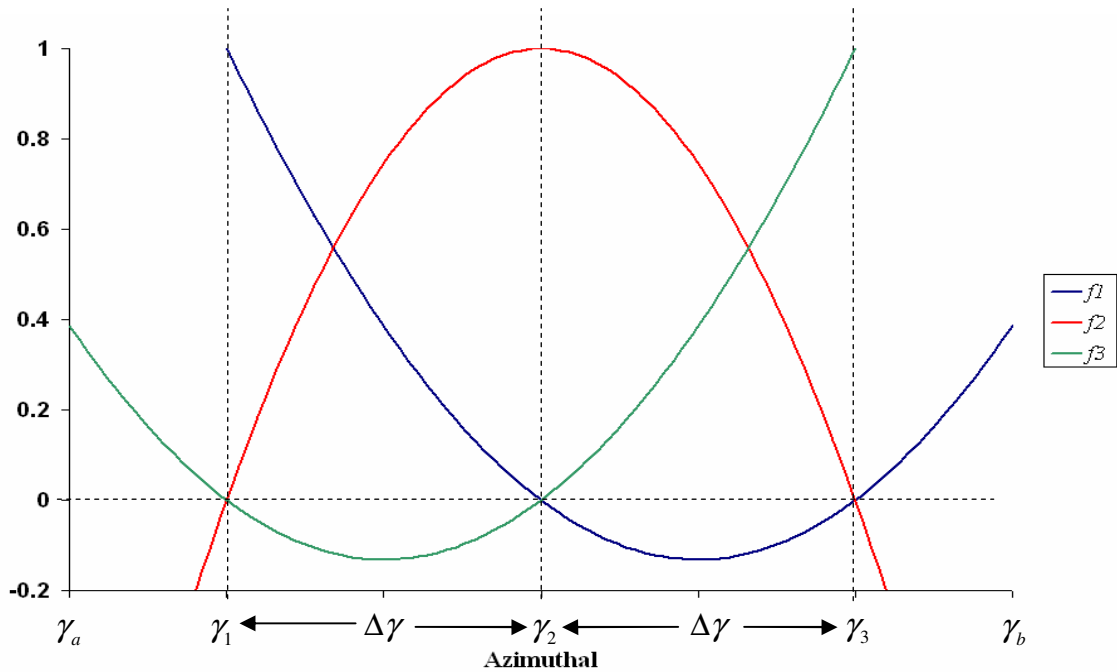
Figure 10 The LSC basis functions.

The LSC weights are calculated by integrating the basis functions over the range $[\gamma_a, \gamma_b]$. The first and third basis functions' integrals are equal on the range $[\gamma_a, \gamma_b]$ as long as $\gamma_b - \gamma_3 = \gamma_1 - \gamma_a$. Note that these basis functions remain well defined if γ_a is equal to γ_1 and/or γ_b is equal to γ_3. The only problem that may occur is negative weights for the middle basis function. This happens when $\Delta\gamma$ is smaller than half the range between γ_1 and γ_a or γ_3 and γ_b:

$$\Delta\gamma < \frac{1}{2}|\gamma_1 - \gamma_a| \text{ or } \Delta\gamma < \frac{1}{2}|\gamma_b - \gamma_3|, \tag{4.18}$$

where $\Delta\gamma = \gamma_2 - \gamma_1 = \gamma_3 - \gamma_2$. To prevent negative weights from occurring we require points to be added between γ_a and γ_1 and/or γ_3 and γ_b if Eq. (4.18) is true.

Every LSC test phase requires that two mid-points be tested simultaneously. If either interpolated value fails the test, then both points are added to the quadrature set. This is to ensure that pairs of quadrature intervals are evenly spaced (on the range of $[\gamma_a, \gamma_b]$).

The LSC is an open rule. As in the linear method above, we must calculate the extrapolated values of LSC. We use the Chebyshev abscissae as our initial quadrature points. Two extrapolated values are tested between the quadrature extremes and the quadrant boundaries. Logic must be inserted in order to prevent a situation from arising that cause the inequalities of Eq. (4.18).

D.3. Derivation of the LSC Basis Functions

We begin with some definitions and shorthand notation:

$$\mu_x = \cos(\gamma_x) \quad \eta_x = \sin(\gamma_x) \quad \eta_{x-y} = \sin(\gamma_x - \gamma_y). \tag{4.19}$$

We then set up the linear system of equations for solving the three constants associated with the first basis function:

$$\begin{pmatrix} \mu_1 & \eta_1 & 1 \\ \mu_2 & \eta_2 & 1 \\ \mu_3 & \eta_3 & 1 \end{pmatrix} \begin{pmatrix} A \\ B \\ C \end{pmatrix} = \begin{pmatrix} 1 \\ 0 \\ 0 \end{pmatrix}. \tag{4.20}$$

As mentioned above the range is $\left[\gamma_1 \ge \gamma_a, \gamma_3 \le \gamma_b \right]$, where

$$\gamma_2 = \frac{1}{2}(\gamma_1 + \gamma_3). \tag{4.21}$$

We use elimination to find the three constants for the function:

$$A = \frac{\eta_3 - \eta_2}{\left[(\mu_3 - \mu_1)(\eta_2 - \eta_1) + (\eta_1 - \eta_3)(\mu_2 - \mu_1) \right]}; \tag{4.22}$$

$$B = \frac{\mu_2 - \mu_3}{\left[(\mu_3 - \mu_1)(\eta_2 - \eta_1) + (\eta_1 - \eta_3)(\mu_2 - \mu_1) \right]}; \tag{4.23}$$

$$C = \frac{\mu_3 \eta_2 - \mu_2 \eta_3}{\left[(\mu_3 - \mu_1)(\eta_2 - \eta_1) + (\eta_1 - \eta_3)(\mu_2 - \mu_1) \right]}. \tag{4.24}$$

Substituting Equations (4.22), (4.23), and (4.24) into (4.17) and simplifying using trigonometric identities yields the first basis function:

$$f_1(\gamma) = \frac{\eta_{3-2} + \eta_{2-\gamma} - \eta_{3-\gamma}}{\eta_{2-1} + \eta_{3-2} - \eta_{3-1}}.$$ (4.25)

The other two basis functions are similarly derived:

$$f_2(\gamma) = \frac{\eta_{\gamma-1} + \eta_{3-\gamma} - \eta_{3-1}}{\eta_{2-1} + \eta_{3-2} - \eta_{3-1}};$$ (4.26)

$$f_3(\gamma) = \frac{\eta_{2-1} + \eta_{\gamma-2} - \eta_{\gamma-1}}{\eta_{2-1} + \eta_{3-2} - \eta_{3-1}}.$$ (4.27)

Integrating these three over the range $[\gamma_a, \gamma_b]$ yields the following weight equations:

$$w_1 = \int_{\gamma_a}^{\gamma_b} f_1(\gamma) d\gamma = \frac{\mu_{\gamma_b-3} - \mu_{\gamma_b-2} - \mu_{\gamma_a-3} + \mu_{\gamma_a-2} + \eta_{3-2}(\gamma_b - \gamma_a)}{\eta_{2-1} + \eta_{3-2} - \eta_{3-1}};$$ (4.28)

$$w_2 = \int_{\gamma_a}^{\gamma_b} f_2(\gamma) d\gamma = \frac{\mu_{3-\gamma_a} - \mu_{\gamma_b-3} + \mu_{\gamma_b-1} - \mu_{1-\gamma_a} - \eta_{3-1}(\gamma_b - \gamma_a)}{\eta_{2-1} + \eta_{3-2} - \eta_{3-1}};$$ (4.29)

$$w_3 = \int_{\gamma_a}^{\gamma_b} f_3(\gamma) d\gamma = \frac{\left(\mu_{\gamma_b-1} - \mu_{\gamma_a-1}\right) + \left(\mu_{2-\gamma_b} - \mu_{2-\gamma_a}\right) + \eta_{2-1}(\gamma_b - \gamma_a)}{\eta_{2-1} + \eta_{1-3} + \eta_{3-2}}.$$ (4.30)

When $\left[\gamma_1 = \gamma_a, \gamma_3 = \gamma_b\right]$, which is the case away from quadrant boundaries, the weight equations can be further simplified:

$$w_{1,3} = \int_{\gamma_1}^{\gamma_3} f_{1,3}\left(\gamma\right) d\gamma = \frac{\Delta\gamma - \eta_{\Delta\gamma}}{1 - \mu_{\Delta\gamma}} \; ; \tag{4.31}$$

$$w_2 = \int_{\gamma_1}^{\gamma_3} f_2\left(\gamma\right) d\gamma = \frac{\eta_{\Delta\gamma} - \Delta\gamma\mu_{\Delta\gamma}}{1 - \mu_{\Delta\gamma}} . \tag{4.32}$$

D.4. Polynomial Error Adapting (PEA)

Our third algorithm refines on the errors in a high-order interpolant of the exiting angular fluxes. Consider an f-weighted azimuthal integral of the angular flux:

$$\int_0^{2\pi} f\left(\gamma\right)\psi\left(\gamma\right) d\gamma \approx \sum_{m=1}^{N_{base}} w_m f_m \psi_m^{comp} + \sum_{n=1}^{N_{adapt}} v_n f_n \varepsilon_n \tag{4.33}$$

The polar integration is suppressed. We have decomposed the flux into two components. The first is a high-order interpolant, ψ_n^{poly}, that passes through the "base" quadrature-point values. The second is an "error" term, ε_n, which we define as the difference between the calculated angular flux (from the iterative sweep), ψ_n^{comp}, and ψ_n^{poly}:

$$\varepsilon_n = \psi_n^{comp} - \psi_n^{poly} \tag{4.34}$$

The base quadrature set is usually designed to achieve exact integration of the high-order interpolating functions, which are usually polynomials in $\sin\gamma$ and $\cos\gamma$. The adaptive quadrature set must therefore be chosen to accurately integrate the "error" term. The error term contains any components of the solution that are not smooth; thus, the adaptive sets are usually based on low-order basis functions. An important point is that any function in the high-order interpolation space will be integrated exactly by the combined base + adaptive quadrature set, because $\varepsilon = 0$ for any such function. Thus, with this method, adaptive refinement does not destroy high-order integration.

We perform the same refinement testing described by Eq. (4.2), but our ψ_n^{int} is now a combination of the polynomial interpolant and the error function interpolant:

$$\psi_n^{int} = \psi_n^{poly} + \varepsilon_n^{int} \tag{4.35}$$

In the results we present below, we interpolate the error function of the polynomial using either the Linear rule (PEAL) or the LSC rule (PEALSC). This means that the weights $\{v_n\}$ of the error term in Eq. 4.33 are generated as described in the Linear and LSC methods. In the first refinement sweep all ε_n^{int} are necessarily zero; thus the first sweep is comparing ψ_n^{poly} directly to ψ_n^{comp}. In all subsequent refinement sweeps, wherever

points have been added to the quadrature set, we compare $\psi_n^{int} = \psi_n^{poly} + \varepsilon_n^{int}$ to ψ_n^{comp}. The higher order interpolant remains unchanged.

It is possible to use other interpolatory function rules (e.g. the Chebyshev polynomials for a global $[0, 2\pi]$ polynomial approximation) as the basis functions for the PEA method. However, in order to maintain the consistency of our quadrant-based quadrature sets, we use the "quadruple-range" quadrature defined by Abu-Shumays.[30] The Abu-Shumays polynomials are briefly mentioned in the previous section. The term quadruple-range "corresponds to subdividing the range of $\gamma \in [0, 2\pi]$ into four equal parts."

As in the previous algorithms, we begin with a base quadrature set. We make our initial iterative sweeps of the problem using the base set. Before we begin the refinement testing, the constants $\{c_j\}$ for the polynomials are calculated and stored for each exiting surface of the boundary cells of each region:

$$\sum_{j=1}^{N_b} c_j b_j\left(\gamma_m^b\right) = \psi_m^b. \tag{4.36}$$

The basis functions $b_j\left(\gamma_m^b\right)$ are provided by Abu-Shumays.[35] The exiting angular flux ψ_m^b is calculated for each angle in the region's quadrature set. The Abu-Shumays' basis functions are:

$$b_j(\gamma) = \begin{cases} \sin^{j-1}(\gamma) & j \neq 3,7,11,15... \\ \sin^{j-2}(\gamma)\cos(\gamma) & j = 3,7,11,15... \end{cases}; \quad \gamma \in \left[0, \frac{\pi}{2}\right]. \qquad (4.37)$$

The j index is the order of the polynomial. For example, if $N_b = 3$, then the polynomial

is:

$$f(\gamma) = c_1 + c_2\sin(\gamma) + c_3\sin(\gamma)\cos(\gamma); \qquad \gamma \in \left[0, \frac{\pi}{2}\right]. \qquad (4.38)$$

The constants $\{c_1, c_2, c_3\}$ are calculated numerically by inverting the basis matrix

B created using the base quadrature set:

$$\begin{pmatrix} b_1(\gamma_1^b) & b_2(\gamma_1^b) & \cdots & b_{N_b}(\gamma_1^b) \\ b_1(\gamma_2^b) & b_2(\gamma_2^b) & \cdots & b_{N_b}(\gamma_2^b) \\ \vdots & \vdots & \vdots & \vdots \\ b_1(\gamma_{N_b}^b) & b_2(\gamma_{N_b}^b) & \cdots & b_{N_b}(\gamma_{N_b}^b) \end{pmatrix} \begin{pmatrix} c_1 \\ c_2 \\ \vdots \\ c_{N_b} \end{pmatrix} = \begin{pmatrix} \psi(\gamma_1^b) \\ \psi(\gamma_2^b) \\ \vdots \\ \psi(\gamma_{N_b}^b) \end{pmatrix}. \qquad (4.39)$$

The inversion of the matrix need only be performed once and stored, since

polynomial order (initial size of the quadrature set N_b) is known from the user input:

$$Bc = \psi \quad \Rightarrow \quad c = B^{-1}\psi. \qquad (4.40)$$

Once the constants are all calculated we are able to calculate the polynomial interpolant of the angular flux anywhere in the quadrant:

$$\psi_n^{poly} = \sum_{j=1}^{N_b} c_j b_j(\gamma_n).$$

(4.41)

The weights of each base quadrature point (w_m) are provided by Abu-Shumays.[35] After each refinement we adjust them on a global basis with the addition of the adapted quadrature points. We substitute Eq. (4.34) into the 0th moment of Eq. (4.33):

$$\int \psi(\gamma) d\gamma \approx \sum_{m=1}^{N_{base}} w_m \psi_m^{comp} + \sum_{n=1}^{N_{adapt}} v_n \left[\psi_n^{comp} - \psi_n^{poly} \right].$$

(4.42)

The adapted quadrature point weights (v_n) are derived from the quadrature rule used for interpolation (linear or LSC). These weights are "folded" into the base weights as follows. We substitute Eq. (4.41) into Eq. (4.42):

$$\int \psi(\gamma) d\gamma \approx \sum_{m=1}^{N_b} w_m \psi_m^{comp} + \sum_{n=1}^{N_a} v_n \psi_n^{comp} - \sum_{n=1}^{N_a} v_n \sum_{j=1}^{N_b} c_j b_j(\gamma_n).$$

(4.43)

We rearrange Eq. (4.36) solving for the constants c_j:

$$c_j = \sum_{m=1}^{N_b} \tilde{b}_j (\gamma_m) \psi_m^{comp} \qquad (4.44)$$

where $\tilde{b}_j$ are elements of the matrix B^{-1}. We substitute Eq. (4.44) into Eq. (4.43):

$$\int \psi (\gamma) d\gamma \approx \sum_{m=1}^{N_b} w_m \psi_m^{comp} + \sum_{n=1}^{N_a} v_n \psi_n^{comp}$$
$$- \sum_{n=1}^{N_a} v_n \sum_{j=1}^{N_b} \left[\sum_{m=1}^{N_b} \tilde{b}_j (\gamma_m) \psi_m^{comp} \right] b_j (\gamma_n). \qquad (4.45)$$

Then we rearrange and combine sums:

$$\int \psi (\gamma) d\gamma \approx \sum_{m=1}^{N_b} \underbrace{\left[w_m - \sum_{n=1}^{N_a} v_n \sum_{j=1}^{N_b} \tilde{b}_j (\gamma_m) b_j (\gamma_n) \right]}_{\tilde{w}_m} \psi_m^{comp} + \sum_{n=1}^{N_a} v_n \psi_n^{comp} . \qquad (4.46)$$

Unlike the previous two adaptive methods the weights no longer depend only on their neighbors. As the number of adapted angles increases, all of the base weights $(\tilde{w}_m)$ change (get smaller). We then use the following modified quadrature set to calculate the scalar flux and update the scattering source:

$$\phi \approx \sum_{m=1}^{N_b} \tilde{w}_m \psi_m^{comp} + \sum_{n=1}^{N_a} v_n \psi_n^{comp} . \qquad (4.47)$$

The weights for higher moments of this rule, such as partial current, have a similar derivation:

$$J \approx \sum_{m=1}^{N_b} \underbrace{\left[w_m \mu_m - \sum_{n=1}^{N_a} v_n \mu_n \sum_{j=1}^{N_b} \tilde{b}_j(\gamma_m) b_j(\gamma_n) \right]}_{\tilde{w}_m} \psi_m^{comp} + \sum_{n=1}^{N_a} v_n \mu_n \psi_n^{comp} \ . \qquad (4.48)$$

E. Program Algorithm

We present here an outline of the algorithm executed by our program:

Input:

- problem geometry, divided into quadrature regions;

- initial quadrature set;

- method of adapting if applicable

- adapting criteria if applicable;

- source convergence criterion

Iterative/Adaptive sweeps:

- refinement tests and modification of quadrature sets (not performed during

  the first iteration);

  ▪ Create a list of test angles for each region from the midpoints from the

    quadrature sets used in the previous iteration;

  ▪ Perform sweeps in direction of particle flow;

- Compare computed exiting angular flux in test directions on region surfaces to interpolated values generated using results computed in the previous iterative sweep.

  - Calculation (non-adaptive) sweep of the problem

    - Use the most recent quadrature set after updating weights at the beginning of each region sweep.

    - Compute the average angular flux in each cell for each quadrature point (each of these cell-averaged angular fluxes is counted as one "unknown") and use the quadrature set to calculate a new scalar flux.

  - Compute the new scattering source for each cell.

  - If there have been no additional quadrature points added from the previous refinement then perform a convergence check.

  - If the check fails then repeat this section.

Conservation sweep:

  - If refinements were made then perform another sweep of the problem, modifying the incident angular flux on each region surface using a scaling factor (see Section 4.C.).

End Algorithm.

F. Memory Requirements

The storage of exiting angular flux on each region boundary can cause the adaptive program to demand a great deal of memory. For our algorithm, these exiting angular

flux values are needed to generate the interpolated values used in the test sweeps. If we store the values in computer memory they can limit the size of our test problems. For our demonstration code we have chosen to save exiting angular flux values in scratch files on the iteration sweep before an adaptive iteration. During the adaptive sweep, we then read only the values that are necessary for a given region in the direction of particle flow; thus reducing much memory load. Writing to and reading from disk slows the analysis somewhat, but for this study we are interested in "proof of principle" rather than programming efficiencies.

G. Summary

We have argued that an efficient placement of quadrature points can greatly increase the accuracy of the transport solution. Although this adds computational expense per unknown, this expense could be amortized over many time steps in a time-dependent problem, or over several iterations in many iterative problems. It also reduces the number of unknowns needed for a given accuracy. We test locally in both position and direction with one of four user-chosen methods (Linear, LSC, PEAL and PEALSC). We force conservation with a scaling factor (a function of exiting and incident partial current) that we calculate on each region boundary. The third and fourth methods of adaptive integration maintain the base interpolative function and thus integrate N_B-order polynomials in $\sin(\gamma)$ and $\cos(\gamma)$. Other interpolative functions could be used in the third/fourth method, but they are not examined in our work. Lastly, in this section we

presented the program algorithm that we utilize in this research and discussed memory

management in the programming process.

V. RESULTS

In this section we show the effectiveness and shortcomings of our research. We start our analysis by examining how our adaptive algorithm performs when it is used to integrate functions for which the analytic answer can be easily determined. Our intent is to show how each of our methods can accurately interpolate and integrate three functions for which the analytic answers are known. Next we examine a simple corner source problem in a purely absorbing material. Ray effects are most clearly visible in the purely absorbing problems. It is our intention to demonstrate how well our adaptive methods can mitigate ray effects. Lastly, we examine two scattering problems with features of practical problems. In problems with "true" rays, errors caused by angular discretization can be difficult to distinguish from the true solution features. Once again, we intend to demonstrate how our methods can find and eliminate these errors to within a user specified tolerance. However, before we begin our analysis, we present an explanation of our analytic process.

A. Definitions of Solution Metrics and Descriptive Notations

In order to more clearly convey how we present our data, we begin with a brief description of our terminology. There are a few shorthand notations that we use when describing the error of our scalar flux. They are used in the figures as well as in the analysis of our data:

Absolute Relative Error (ARE) is:

$$ARE = \frac{\left| x_{ref} - x_{soln} \right|}{\left| x_{ref} \right|} \tag{5.1}$$

where $\{ x_{ref} \}$ is the reference solution (where practical we compute the analytic solution

of the problem with double precision accuracy; however, on our large problems we

generate the reference using a very fine uniform quadrature set); and $\{ x_{soln} \}$ is the

solution computed to some tolerance set by the user.

We define RMS, Eq. (5.2) as the square root of the average square of the absolute

relative error of the computed scalar flux, $\{ \phi^{Comp} \}$ with respect to the reference scalar

flux, $\{ \phi^{REF} \}$ averaged over N_{cells} spatial cells. We define this weighted norm in order to

analyze problems with a wide range of scalar flux magnitudes (because ϕ can vary by

several orders of magnitude).

$$RMS = \sqrt{\frac{\displaystyle\sum_{n=1}^{N_{cells}} \frac{\left| \phi_n^{REF} - \phi_n^{Comp} \right|^2}{\left| \phi_n^{REF} \right|^2}}{N_{cells}}} \tag{5.2}$$

EQSP is a quadrature set with equally spaced abscissa. They are the Chebyshev

quadrature points:

$$\gamma_n(q) = \frac{(2n-1)\pi}{4N_B} + (q-1)\frac{\pi}{2}; \quad n = 1,\ldots,N_B; \quad q = 1,\ldots,4, \tag{5.3}$$

where N_B is the number of azimuthal angles $\{\gamma_n\}$ per quadrant. For example, LSC 9 EQSP is weighting method LSC with 9 equally spaced angles per quadrant. If it is preceded by "Linear" then the weights are the Chebyshev weights:

$$w = \frac{\pi}{2N_B} \tag{5.4}$$

If it is preceded by "LSC" then the weights are calculated using the derivations described in Section 4.D.2. A quadrature rule name (Linear, LSC, PEAL or PEALSC) followed by a number is an adaptive method. The number designates the starting size (N_B) (i.e. before refinement) of the quadrature set (e.g. LSC9 is the LSC adaptive quadrature rule that begins with 9 EQSP quadrature points per quadrant). We say that a quadrature set is even or odd in the case of the Linear method if N_B is even or odd; in the case of the LSC method if n is even or odd in Eq. 5.5 for the number of base points per quadrant, N_B then the LSC method is even or odd:

$$N_B = 2n+1 \quad n = 1,2,\ldots \tag{5.5}$$

Thus, LSC-7 is "odd" and LSC-9 is "even," for example.

B. An Outline of Our Presentation of Data

In the list below we explain the various ways that we analyze the data that we collect from our research. These are just a few of the many ways one could present the data.

- We plot scalar flux vs. position along a problem's boundary edge to show the oscillations caused by ray effects, or their elimination.

- We plot scalar flux vs. position on a 2D pseudo-color plane to show the oscillations due to ray effects or the elimination of the ray effects.

- We plot angular flux vs. azimuthal angle from an exiting surface of a cell. This plot is designed to show the region/cell with the most drastic peak and to show the region/cell where the test failed most often (i.e. added the most new quadrature points).

- We plot RMS (or ARE where appropriate) vs. unknowns to illustrate how well the method we are examining is converging and how many fewer adapted unknowns are needed for a given accuracy. We also add a trend line and equation, where appropriate.

C. Minimum Allowable Δγ

An algorithm parameter that has not been mentioned thus far is the minimum allowable azimuthal width between two quadrature points (min_DG). Without such a parameter, Gibb's phenomenon (oscillations of interpolated solutions near discontinuities) causes our algorithm to refine indefinitely in the neighborhood of a

solution discontinuity or near-discontinuity. This is because our refinement test is point-wise, not integral, and any high-order interpolation will over- or under-shoot the solution at the quadrature test points that are nearest the discontinuity, no matter how closely spaced the points are. The value of min_DG has been fixed at 0.02 radians for most of our test problems; however we vary it in certain problems to allow the adaptive algorithm to try to resolve "jump" discontinuities (as in function 3 below). If the min_DG is not allowed to vary then our adaptive algorithm would not be able to produce an arbitrarily small integration error, because it would stop refining at some maximum number of quadrature points regardless of the adapting criteria (ε_{th} and ε_{ψ}). If the min_DG is set to zero then the adapting process never ceases at the "jump" discontinuities. Our algorithm has no other way to account for a "jump" discontinuity at this time; and, other than adding many points to the range around a "jump" discontinuity, it has no way to mitigate the effects of Gibb's phenomena. A possible alternative for future consideration is to base refinement decisions on integrals over sub-intervals instead of on point values. Another is to switch to linear interpolation once a threshold $\Delta\gamma$ is reached.

D. A 6th Order Polynomial Function in the Azimuthal Angle

We examine here some functions of azimuthal angle on the range $\left[0, \dfrac{\pi}{2}\right]$. The first function (Figure 11) is a 6th-order polynomial.
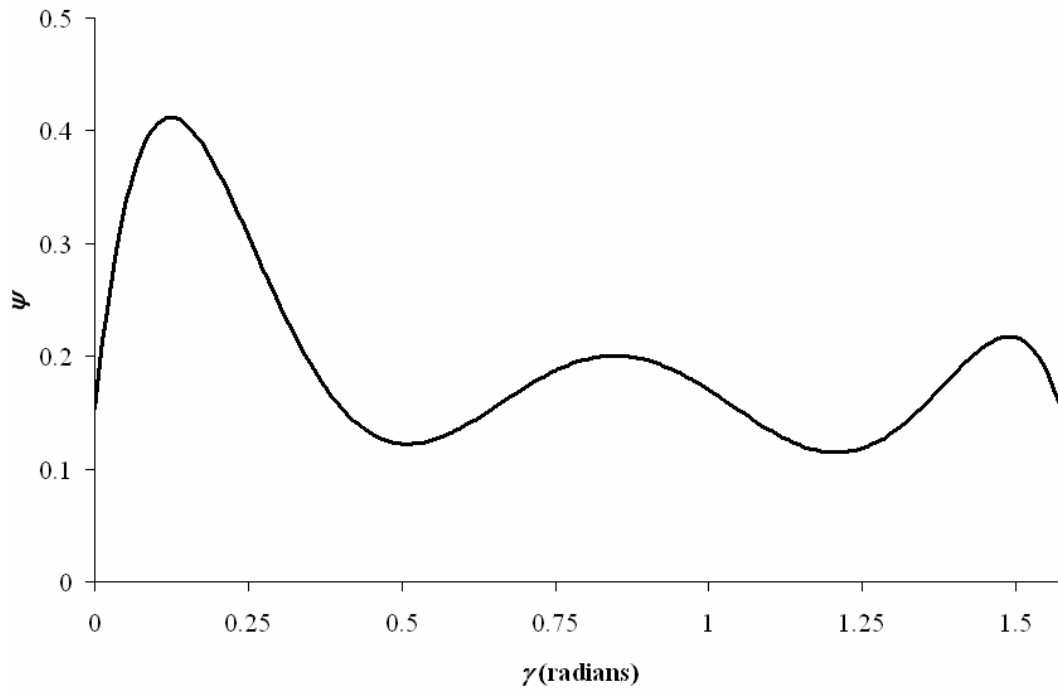
Figure 11   A 6th-order polynomial function on the range $\left[0, \dfrac{\pi}{2}\right]$.

The equation of the polynomial function is:

$$\psi(\gamma) = -8.75\gamma^6 + 43.9\gamma^5 - 83.9\gamma^4 + 75.9\gamma^3 - 32.1\gamma^2 + 5.06\gamma + 0.153 . \qquad (5.6)$$

The integral of the polynomial is:

$$\int_0^{\frac{\pi}{2}} d\gamma\, \psi(\gamma) \cong 0.309997 . \qquad (5.7)$$

Figure 12, Figure 13, Figure 14 and Figure 15 display plots of absolute relative error (between the analytic and computed solutions) as a function of the number of quadrature points (needed to achieve a given user-input refinement criteria). The interpolation tolerance (ε_ψ) is initially set to 10% and adjusts downward to 0.001% for independent runs. The threshold tolerance (ε_{th}) is initially set at 1% and automatically adjusts downward by one order of magnitude if the adaptive process stops before the convergence criteria is satisfied; thus allowing more angles to be added that previously were rejected as "insignificant." The min_DG is also allowed to vary downward (from .02 radians to .001 radians) if the accuracy does not improve as the number of quadrature points increase. The adaptive method used in each figure is Linear, PEAL, LSC and PEALSC, respectively. In the figures using a linear method for adapting, a set of EQSP Linear solutions are shown (Figure 12 and Figure 13). In those showing the LSC adapting methods (Figure 14 and Figure 15), a set of EQSP LSC solutions are shown. Four initial quadrature sets are run for each method (two "even" and two "odd"). The reason for the even and odd starting quadrature sets arose from the difference in the accuracy noticed in the EQSP quadrature sets while examining the exponential cusp function. It is explained more clearly in the description and analysis of the exponential cusp function (below). A linear trendline is included to indicate the overall convergence of the adaptive solutions.
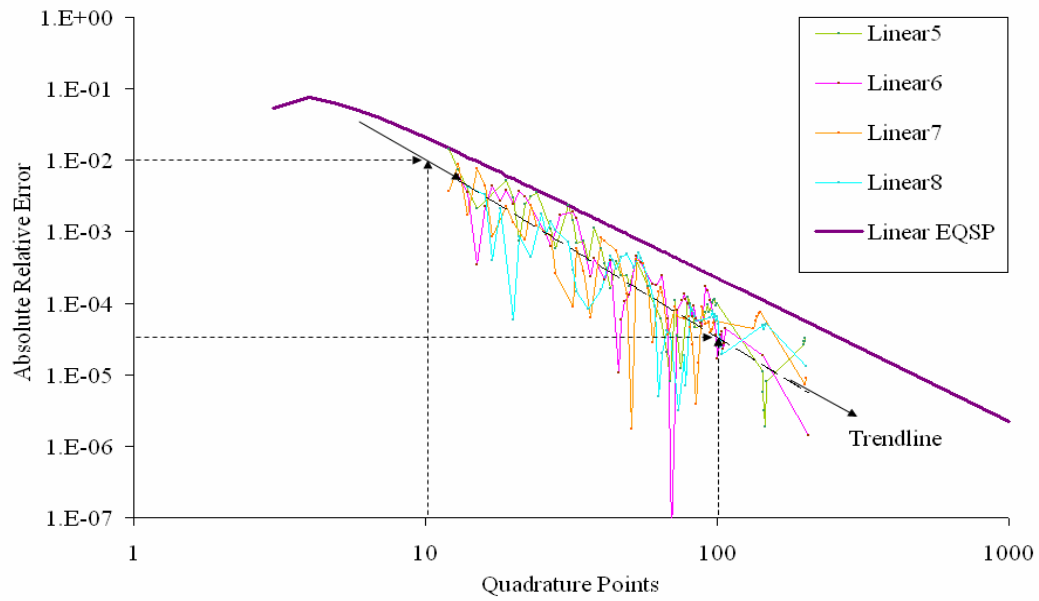
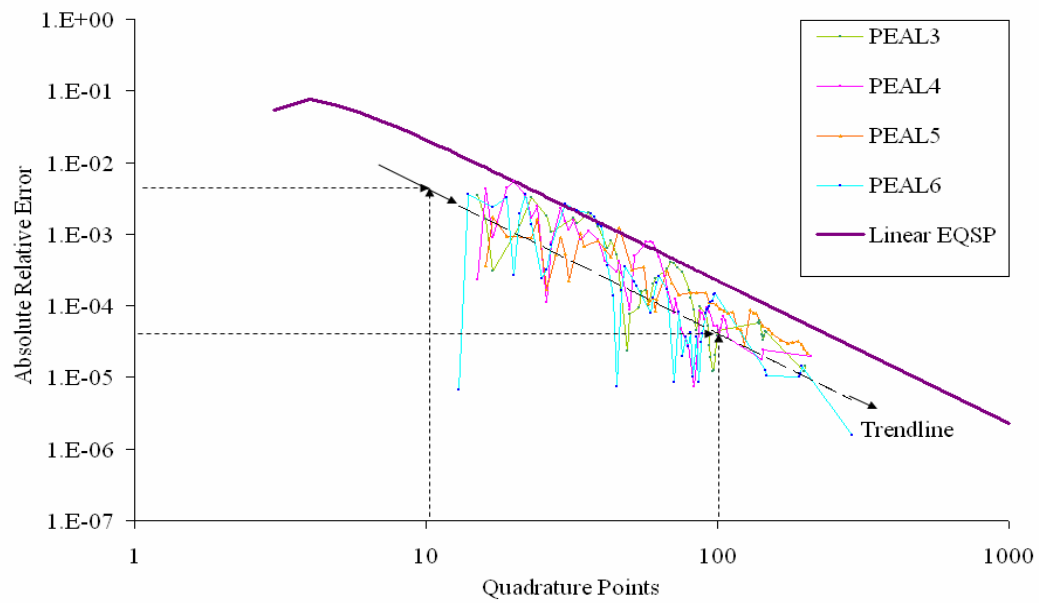Figure 12   Linear adaptive performances for the 6th order polynomial.

Figure 13   PEAL adaptive performances for the 6th order polynomial.
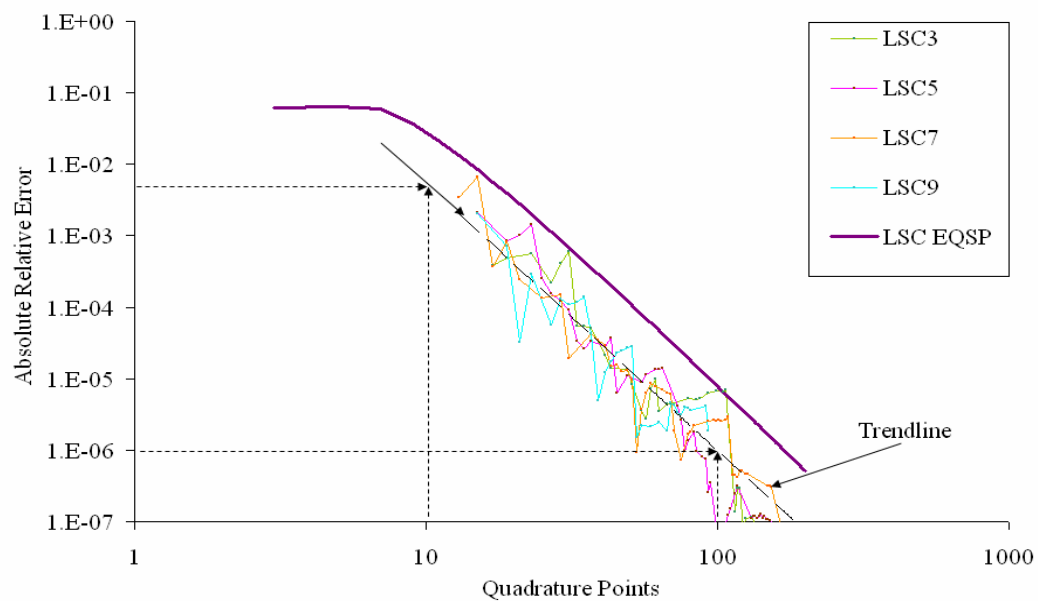
Figure 14   LSC adaptive performances for the 6th order polynomial.
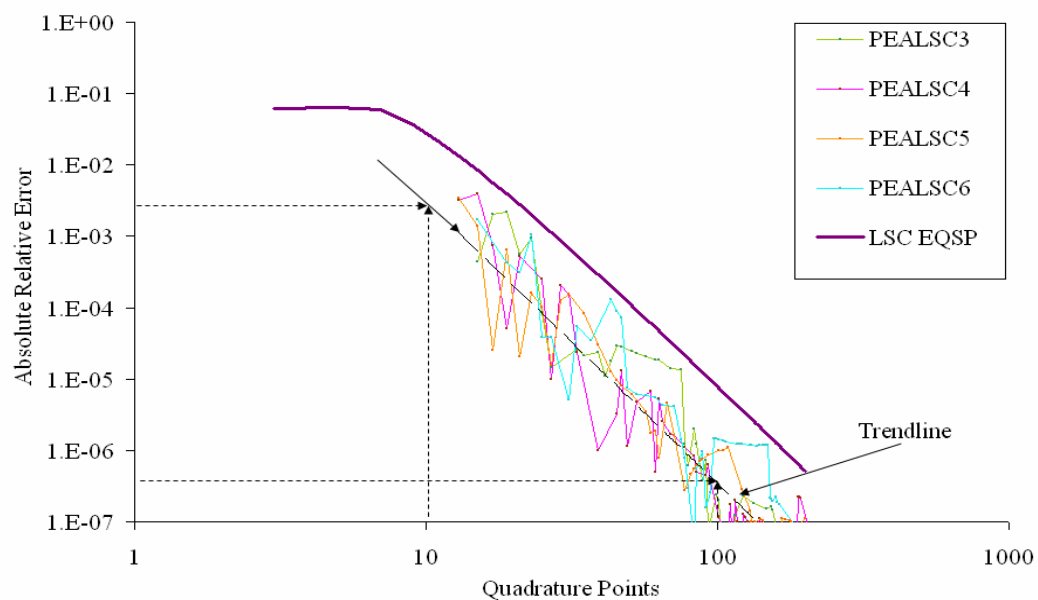

Figure 15   PEALSC adaptive performances for the 6th order polynomial.

As can be seen from the graphs above, the overall accuracy is improved by using any of the adaptive methods (note the trendline vs. the EQSP solution line). The lines with color drawn in the figures connect the ARE points for a given quadrature set (adaptive and EQSP). Some of the adaptive solutions are several orders of magnitude better than the corresponding EQSP quadrature set. We do not have any additional logic in our algorithm to determine which adapted quadrature set is sufficient. Our algorithm is totally dependent on the accuracy of the interpolation of the function.

In the linear methods (Linear and PEAL), accuracy is improved by approximately one order of magnitude over the EQSP Linear solutions for a given number of quadrature points. The LSC methods (LSC and PEALSC) perform even better with approximately one and a half order magnitude improvement in accuracy for a given number of quadrature points. Other than Linear Adaptive vs. Linear EQSP (Figure 12), there are no marked improvements over convergence rates. The EQSP Linear is $O\left(\frac{1}{N}\right)^2$ and the EQSP LSC is $O\left(\frac{1}{N}\right)^4$, according to the plots. The trendlines for the adaptive methods indicate $O\left(\frac{1}{N}\right)^3$ for Linear, $O\left(\frac{1}{N}\right)^2$ for PEAL, $O\left(\frac{1}{N}\right)^4$ for LSC and $O\left(\frac{1}{N}\right)^4$ for PEALSC.

D. The Exponential Cusp-Shape Function

The second problem we examine is an exponential cusp-shaped function (plotted in Figure 16). The function is symmetric around the cusp (discontinuity in the first derivative), which is located at $\pi/4$.
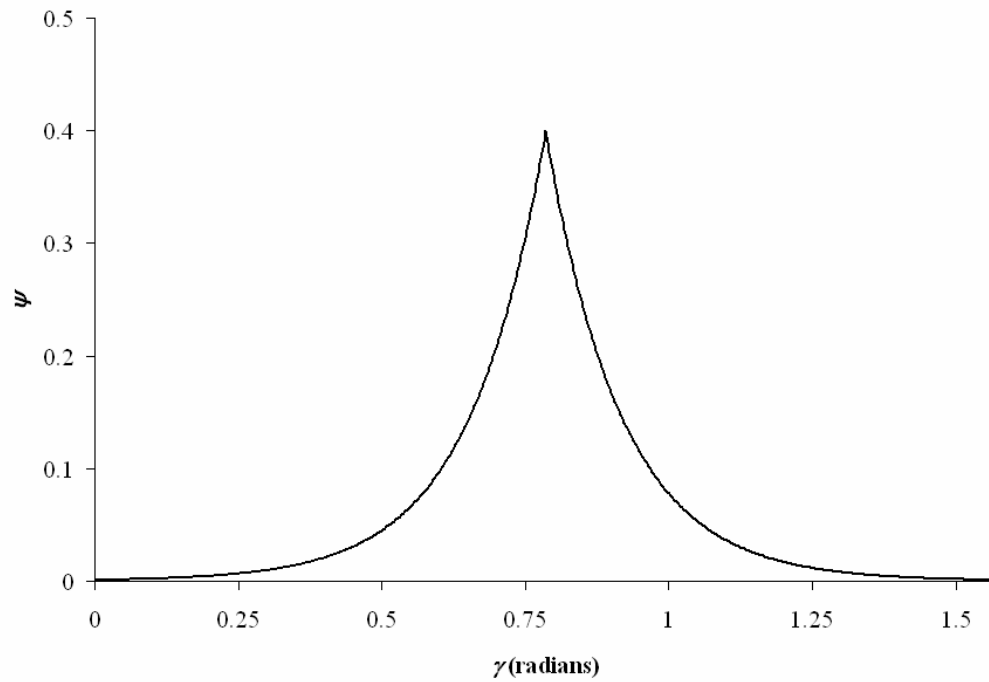
Figure 16   An exponential cusp function on the range $[0, \pi/2]$.

The equation of the exponential function is:

$$\psi(\gamma) = 0.4e^{\left(7.63\left|\gamma - \frac{\pi}{4}\right|\right)}$$

(5.8)

The integral of the exponential is:

$$\int_{0}^{\frac{\pi}{2}} d\gamma \psi(\gamma) \cong 0.1046$$

(5.9)

Figure 17, Figure 18, Figure 19 and Figure 20 display plots of absolute relative error (between the analytic and computed solutions) versus the number of quadrature points necessary for a given user-input refinement criteria (ε_ψ and ε_{th}). The interpolation tolerance (ε_ψ) is initially set to 10% and adjusts downward to 0.001% for independent runs. The threshold tolerance (ε_{th}) is initially set at 1% and automatically adjusts downward by one order of magnitude if the adaptive process stops before the convergence criteria is satisfied; thus allowing more angles to be added that previously were rejected as "insignificant." The min_DG is also allowed to vary downward (from .02 radians to .001 radians) if the accuracy does not improve as the number of quadrature points increase. The adaptive method used in each figure is Linear, PEAL, LSC and PEALSC, respectively. In the figures using a linear method for adapting, two sets of EQSP Linear solutions (one with "even" sized quadrature sets and one with "odd" sized quadrature sets) are shown (Figure 17 and Figure 18). In those showing the LSC adapting methods (Figure 19 and Figure 20), two sets EQSP LSC solutions (one with "even" sized quadrature sets and one with "odd" sized quadrature sets) are shown. Four initial quadrature sets are run for each method (two "even" and two "odd"). There is little variance in the resulting solutions compared with the polynomial function analysis; therefore we do not include a linear trendline.
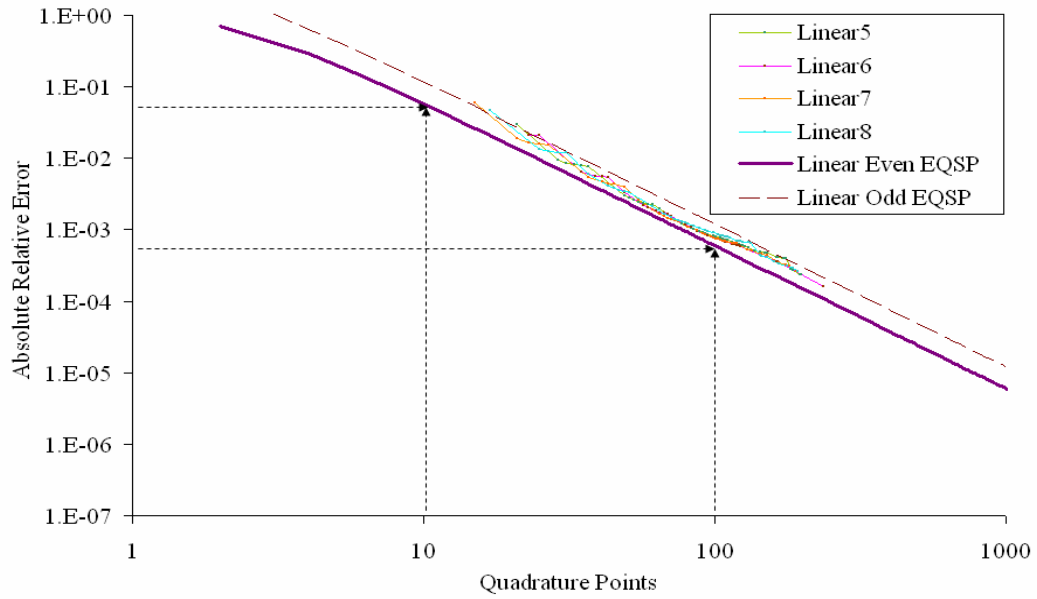
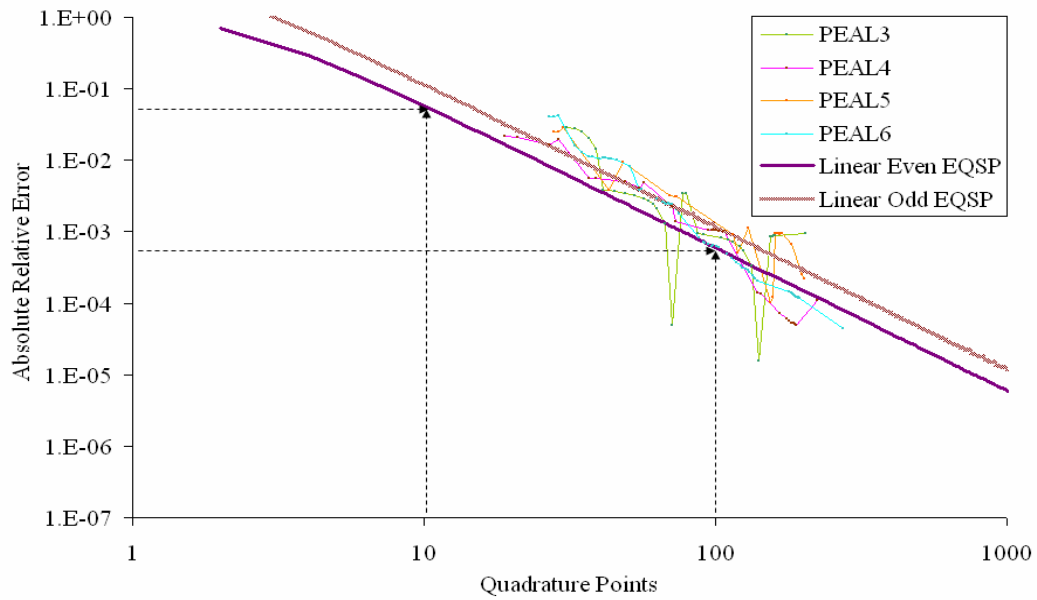Figure 17   Linear adaptive performances for the cusp function.

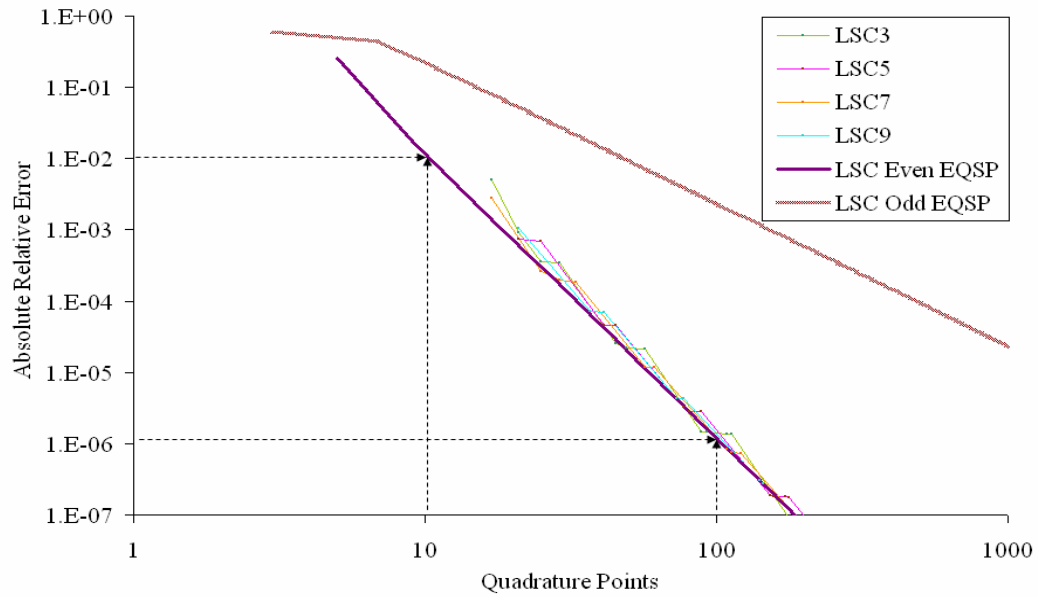Figure 18   PEAL adaptive performances for the cusp function.

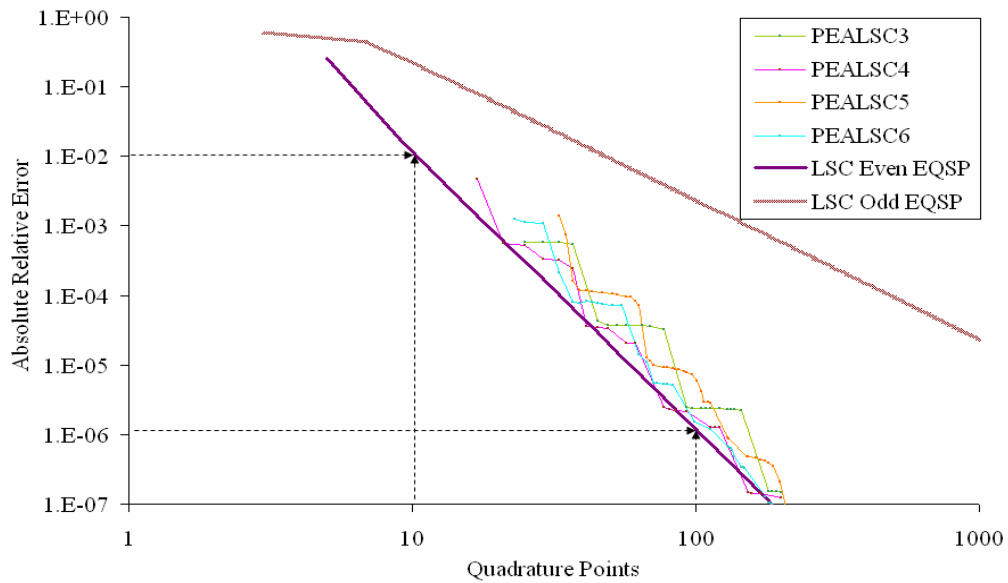Figure 19   LSC adaptive performances for the cusp function.

Figure 20   PEALSC adaptive performances for the cusp function.

The most obvious property that we notice is that the rate of convergence is quite different for even and odd EQSP LSC quadrature sets (see Figures 18 and 19). If we shift the location of the cusp away from $\pi/4$, the difference goes away. The common relationship that all Linear EQSP even quadrature sets share is that none of them have a point at $\pi/4$. For LSC, all quadrature sets have a point at $\pi/4$. However, the point at $\pi/4$ is a *middle* basis-function point for odd quadrature sets but an *edge* basis-function point for even sets (see Figure 10 in Section 4). Thus, the EQSP LSC odd quadrature sets contain an underlying assumption of smoothness at $\pi/4$, whereas the even sets assume only continuity. This appears to be a phenomenon unique to the cusp problem and problems with similar solution behavior. We discuss it here because of its similarities with some of our later transport test problems. The Step-characteristic spatial discretization on rectangular grids in Cartesian geometry causes anomalies in the solution along the quadrant boundaries and along cell-diagonal directions (which for square cells are odd multiples of $\pi/4$). These anomalies introduce cusp-like features in the angular flux, which in turn lead to fundamentally different performance of "even" and "odd" EQSP quadrature sets. However, our results show that no matter what size quadrature set one chooses to begin with, the accuracy and convergence of our adaptive methods are not affected by shape of the function. In fact all adaptive methods are more accurate than the EQSP odd quadrature sets. Linear adaptive and LSC adaptive match the accuracy and convergence of the EQSP even. The PEA methods perform better than the EQSP odd sets but not as well as the EQSP even sets.

E. A Jump Discontinuous Function

The third function (Figure 21) is a polynomial in $\sin(\gamma)$ and $\cos(\gamma)$ with "jump"

discontinuities at 1.0 and 1.4 radians. This type of problem (with sharp peaks or

discontinuities) poses a difficult challenge for quadratures sets for obvious reasons and is

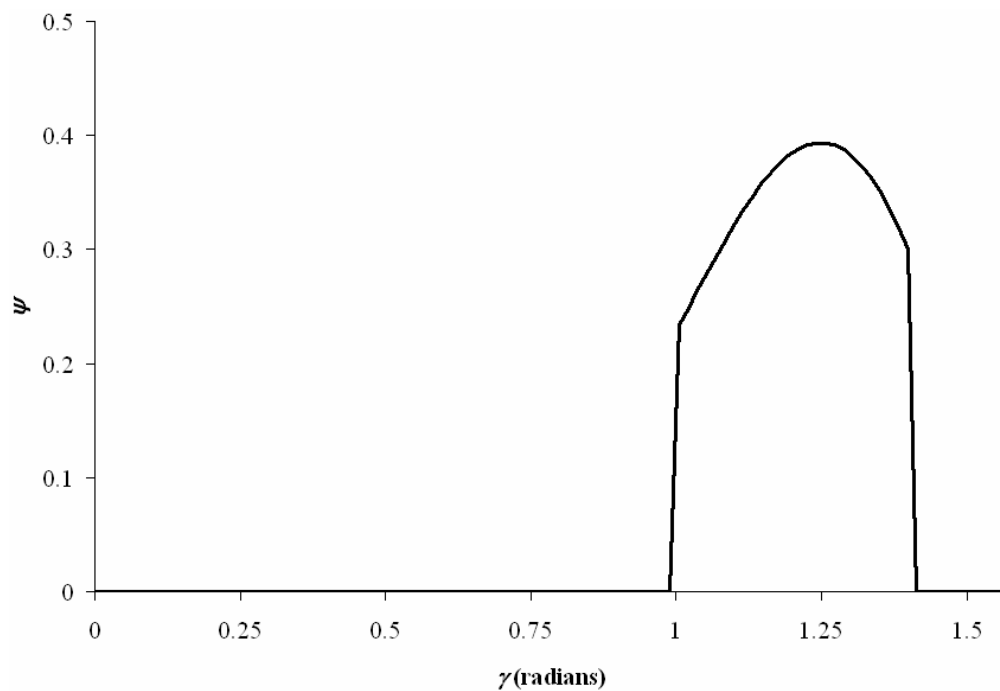one of the motivations we discuss in the first section.

Figure 21   A piecewise polynomial function in $\sin(\gamma)$ and $\cos(\gamma)$ on the range $[0, \pi/2]$.

The equation of the function is:

$$\psi(\gamma) = \begin{cases} 2\sin^9(\gamma)\cos(\gamma) & 1.0 \leq \gamma \leq 1.4 \\ 0 & \text{otherwise} \end{cases} \tag{5.10}$$

The integral of the polynomial in sin and cos function is:

$$\int_{1.0}^{1.4} d\gamma\psi(\gamma) \cong 0.137135 \qquad (5.11)$$

Figure 22, Figure 23, Figure 24 and Figure 25 display plots of absolute relative error (between the analytic and computed solutions) versus the number of quadrature points necessary for a given user-input refinement criteria (ε_ψ and ε_{th}). The interpolation tolerance (ε_ψ) is initially set to 10% and adjusts downward to 0.001% for independent runs. The threshold tolerance (ε_{th}) is initially set at 1% and automatically adjusts downward by one order of magnitude if the adaptive process stops before the convergence criteria is satisfied; thus allowing more angles to be added that previously were rejected as "insignificant." The min_DG is also allowed to vary downward (from .02 radians to .001 radians) if the accuracy does not improve as the number of quadrature points increase. The adaptive method used in each figure is Linear, PEAL, LSC and PEALSC, respectively. In the figures using a linear method for adapting a set of EQSP Linear solutions are shown (Figure 22 and Figure 23). In those showing the LSC adapting methods (Figure 24 and Figure 25), a set of EQSP LSC solutions are shown. Four initial quadrature sets are run for each method (two "even" and two "odd"). A linear trendline is included to indicate the overall convergence of the adaptive solutions.
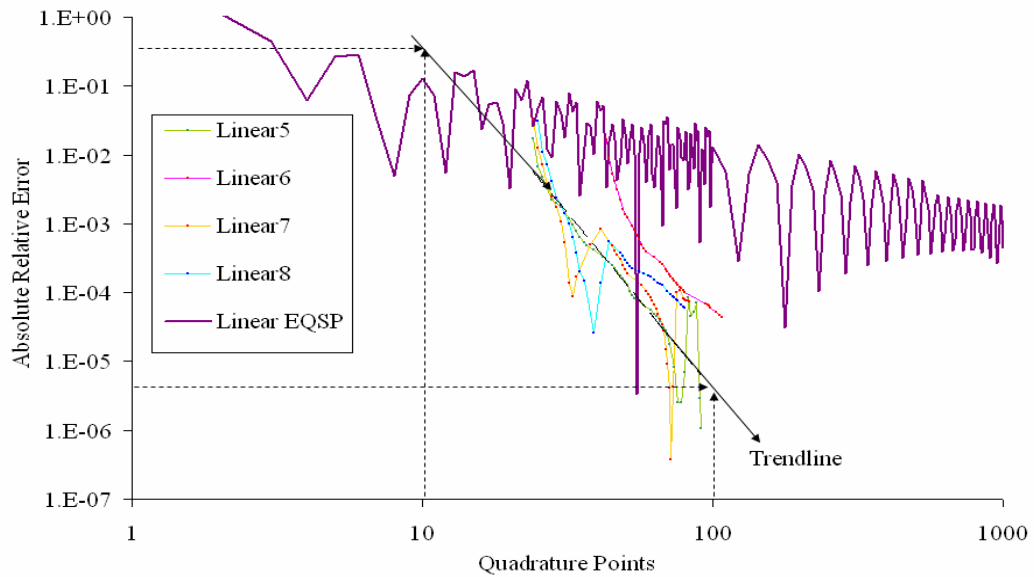
Figure 22   Linear adaptive performances for the polynomial in $\sin(\gamma)$ and $\cos(\gamma)$ with "jump" discontinuities.
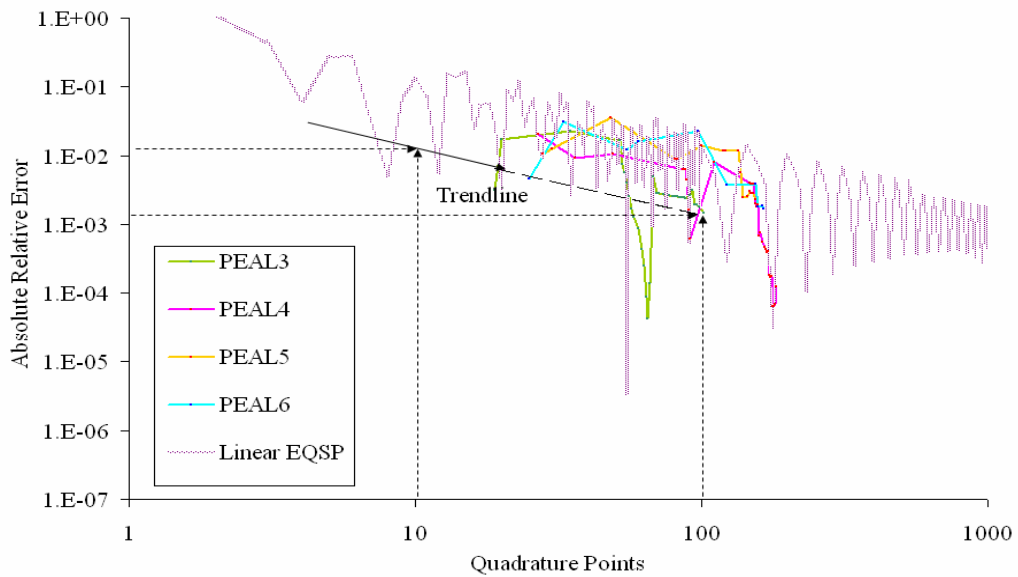

Figure 23   PEAL adaptive performances for the polynomial in $\sin(\gamma)$ and $\cos(\gamma)$ with "jump" discontinuities.
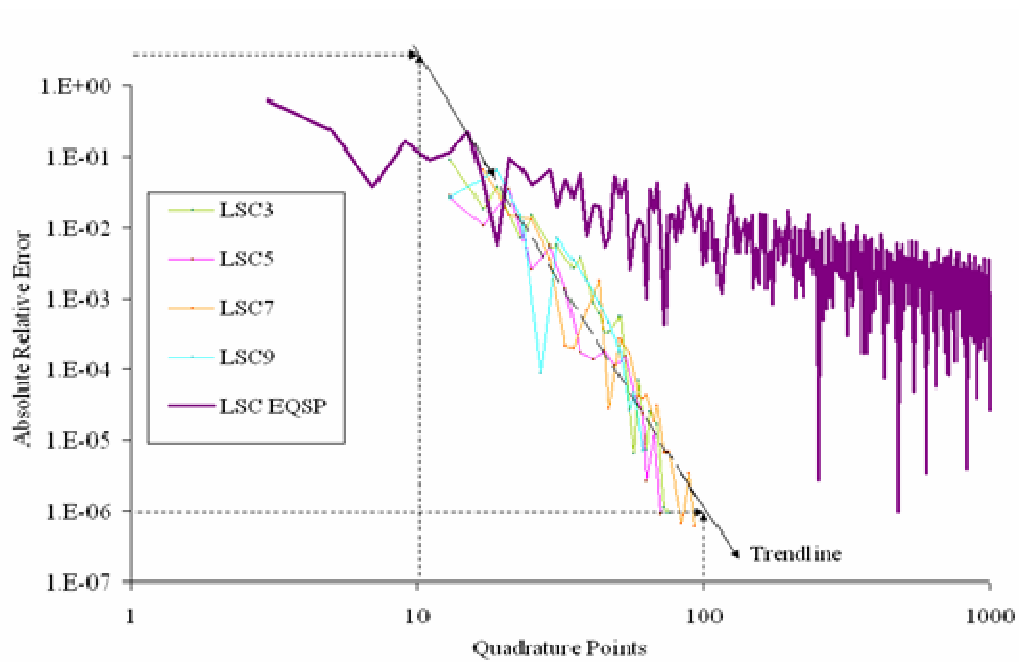
Figure 24   LSC adaptive performances for the polynomial in $\sin(\gamma)$ and $\cos(\gamma)$ with "jump" discontinuities.
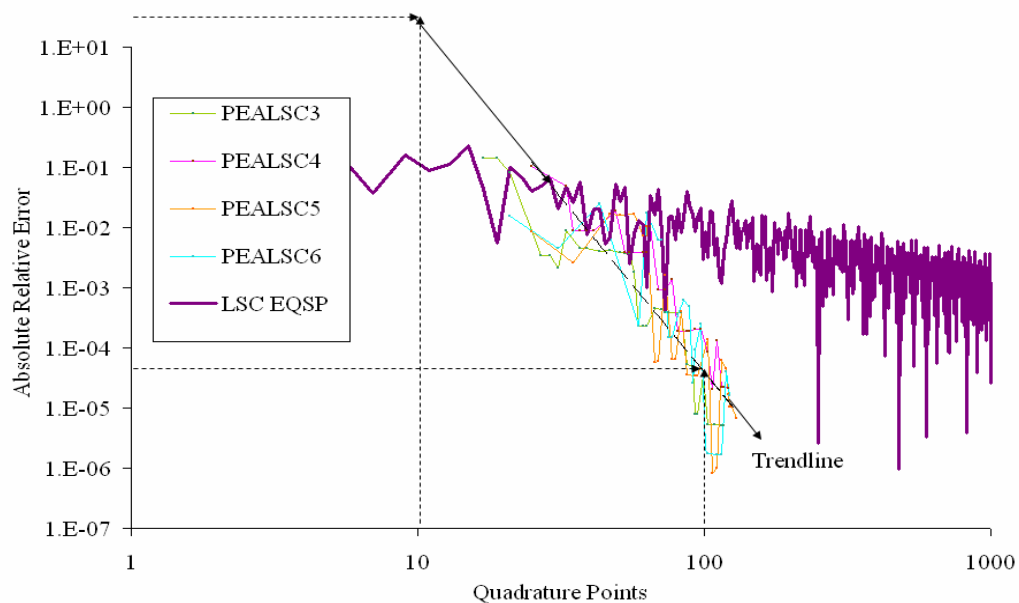

Figure 25   PEALSC adaptive performances for the polynomial in $\sin(\gamma)$ and $\cos(\gamma)$ with "jump" discontinuities.

The difficulty of using an EQSP quadrature set is clearly illustrated in the preceding figures. The accuracy oscillates dramatically and the convergence rate is just better than $O\left(\frac{1}{N}\right)$. Only PEAL of the four adaptive methods fail to outperform the EQSP quadrature sets. In fact, the other three adaptive methods perform quite well on this problem in both accuracy and convergence. The Linear adaptive method has $O\left(\frac{1}{N}\right)^4$ convergence; LSC has $O\left(\frac{1}{N}\right)^6$ convergence; and PEALSC has $O\left(\frac{1}{N}\right)^5$ convergence.

F. Corner Source in a Purely Absorbing Material

Ray effects are most dramatic in purely absorbing problems. Therefore the first two-dimensional problem we examine has a corner source placed in a purely absorbing ($\sigma_t = 0.1$ cm^{-1}) medium shown in Figure 26.
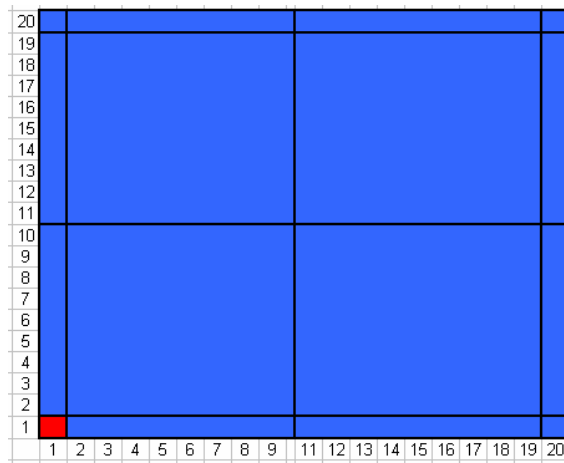

Figure 26   A 20 cm by 20 cm purely absorbing material (blue) with a 1 cm by 1 cm isotropic external source (red) located in the lower left corner – "the corner source."

We divide the surface into 16 "quadrature regions" separated by the dark lines. Each region is sub-divided into cells (1mm by 1mm, resulting in a 200 by 200 spatial grid). Figure 27, Figure 28 and Figure 29 show an LSC9 solution before refinement, after 2 refinement steps, and after all refinement has completed (7 steps). The interpolation tolerance (ε_ψ) is .01% and the threshold tolerance (ε_ψ) is .01%. The min_DG is fixed at .02 radians.
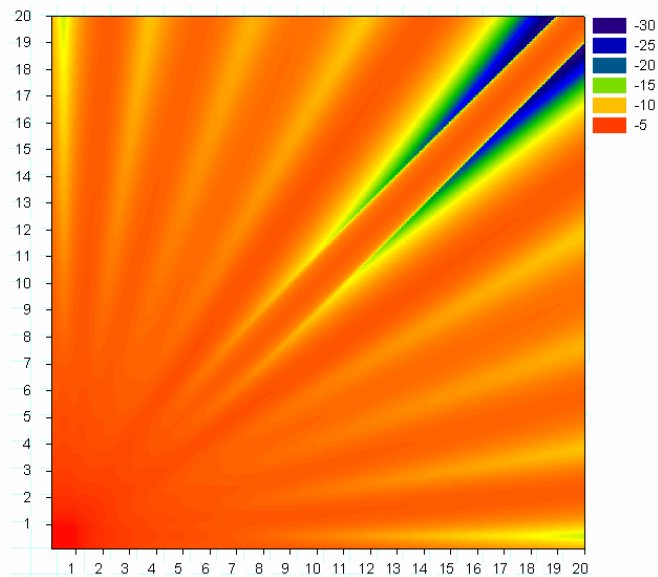

Figure 27   The LSC9 scalar flux for the corner source problem, with no refinement. The legend is in powers of 10. The axes labels are in cm.
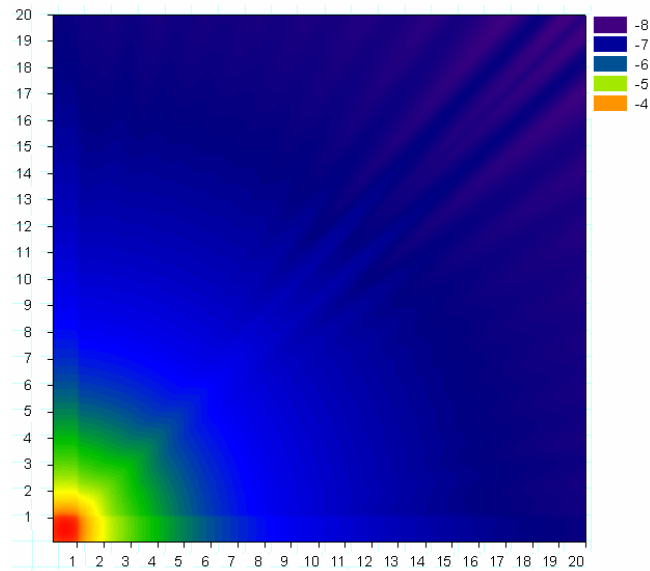
Figure 28   The scalar flux for the corner source problem after 2 refinements. The legend is in powers of 10. The axes labels are in cm.
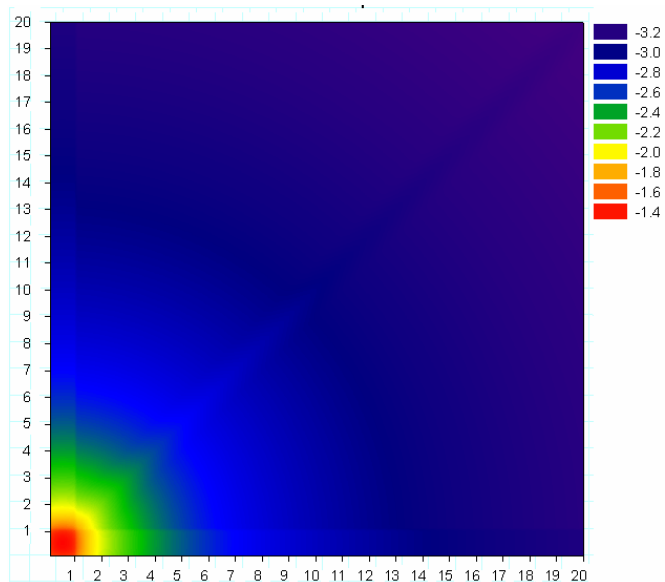

Figure 29   The scalar flux for the corner source problem after all refinements. The legend is in powers of 10. The axes labels are in cm.

The adaptive program eliminates the ray effects from the pseudo-color plots. (The

lack of smoothness in the scalar flux in Figure 29 is entirely due to the step-characteristic

spatial discretization.) The values in the preceding legends are base-10 logarithm of the

solution.

   To illustrate how ordinary quadrature sets are inadequate in performing integration

for this problem, we examine the oscillations of the scalar flux along the rightmost

column of cells (at x = 19.95 cm). A coarse EQSP LSC 9 solution is shown in Figure 30

(also see Figure 27 for the EQSP LSC 9 in the pseudo color plane). A finer EQSP LSC

33 is shown in Figure 31 and is directly compared to the LSC 9 adaptive result shown in

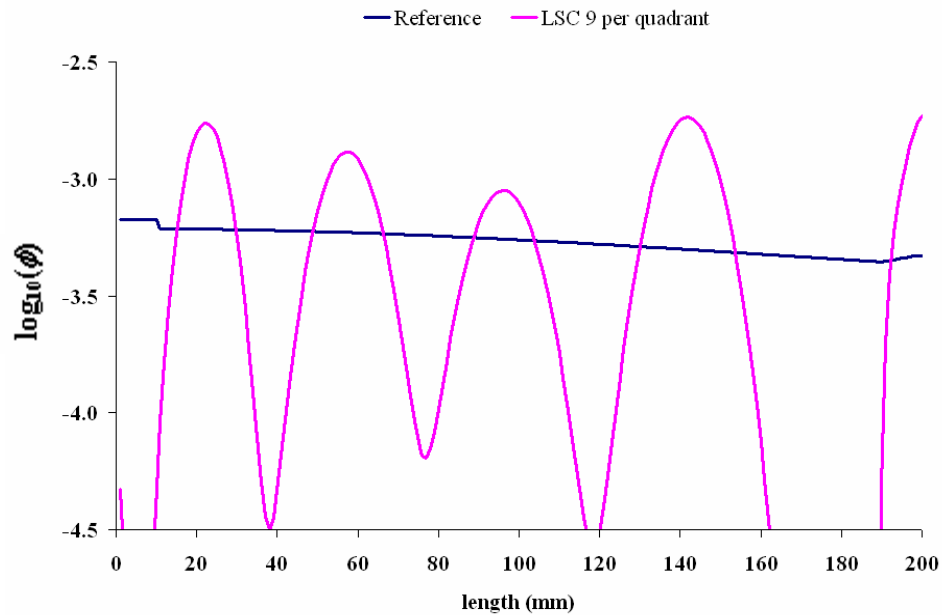Figure 32. The reference solution uses LSC 2001 EQSP.

Figure 30   The scalar flux (phi) solution using LSC 9 EQSP along the outer edge of the
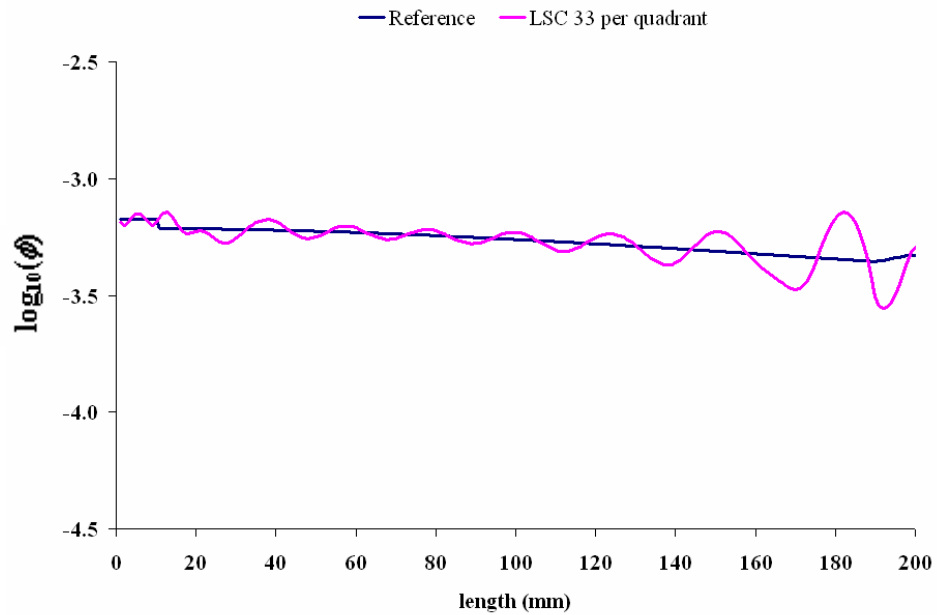corner source problem.

Figure 31   The scalar flux (phi) solution using LSC 33 EQSP along the outer edge of the corner source problem.
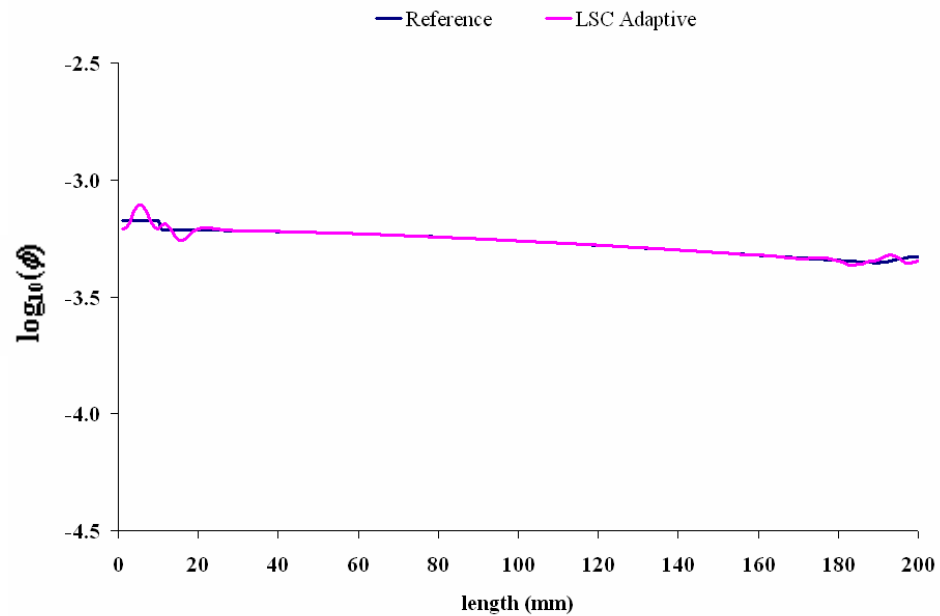

Figure 32   The scalar flux (phi) solution using LSC 9 Adaptive along the outer edge of the corner source problem.

The solution to the corner source problem using LSC 33 EQSP (Figure 31) needs over 5 million unknowns, and ray effects are still obvious. The much more accurate solution using LSC 9 Adaptive (Figure 32) needs approximately 3 million unknowns, and ray effects are significantly mitigated (see Figure 29). The oscillations at the ends (less than 10 mm and greater than 190 mm) are a result of the difficult integration of the spatial anomalies (arising from the step-characteristic spatial discretization). The square shape spatial anomaly in the reference solution (less than 10 mm) is due to the integration of a half cusp function. The slanted spatial anomaly in the reference solution (greater than 190 mm) is due to the integration of function with a full cusp shape.

As with the one-dimensional problems, it is also noteworthy to examine how the adaptive programming can perform with changing user tolerance criteria by plotting RMS vs. unknowns to examine accuracy and convergence over the whole problem. Figure 33 and Figure 34 show how the solution RMS changes when different starting quadrature sets are used. The threshold tolerance is zero in both figures. The angular flux tolerance is varied downward from 1.0% to 0.001%. The zigzag effects of the cusp function can be seen in the EQSP comparison lines. Also, the effects of a fixed min_DG of 0.02 radians can be seen in the sharp "knee" in Figure 33.
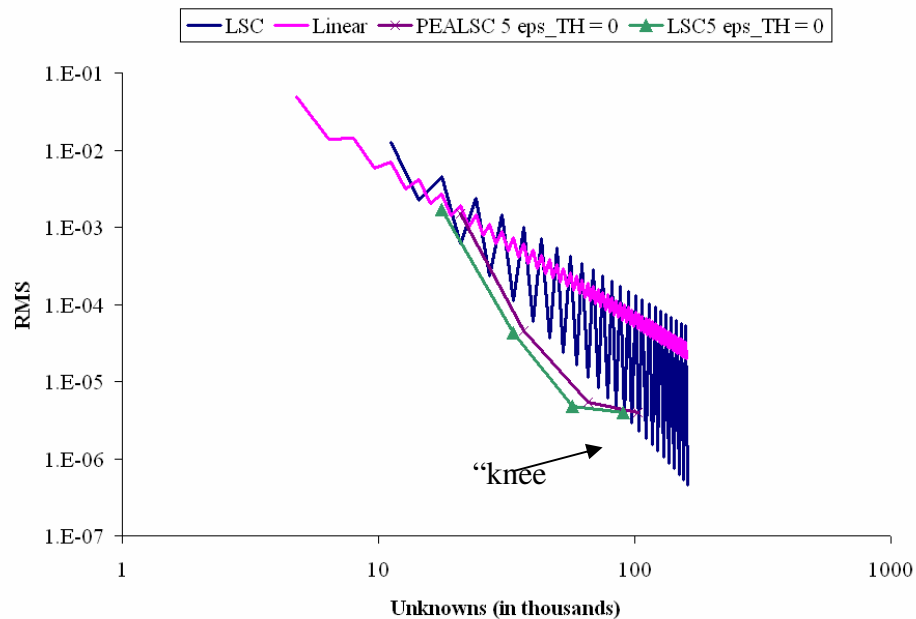
Figure 33   The RMS error in scalar fluxes from EQSP and Adaptive (LSC5 and PEALSC5) methods on the corner source problem.

The "knee" is not as noticeable in Figure 34 (it is much lower on the RMS scale) because we start with a larger quadrature set. The smaller quadrature set performs as well as the larger quadrature set near the source (i.e. within user specified tolerances). However, the larger quadrature set contains angles that are needed farther from the source in order to produce more accurate results around discontinuities. Alternatively, we could also adjust the min_DG value to allow for more refinements around the discontinuities.
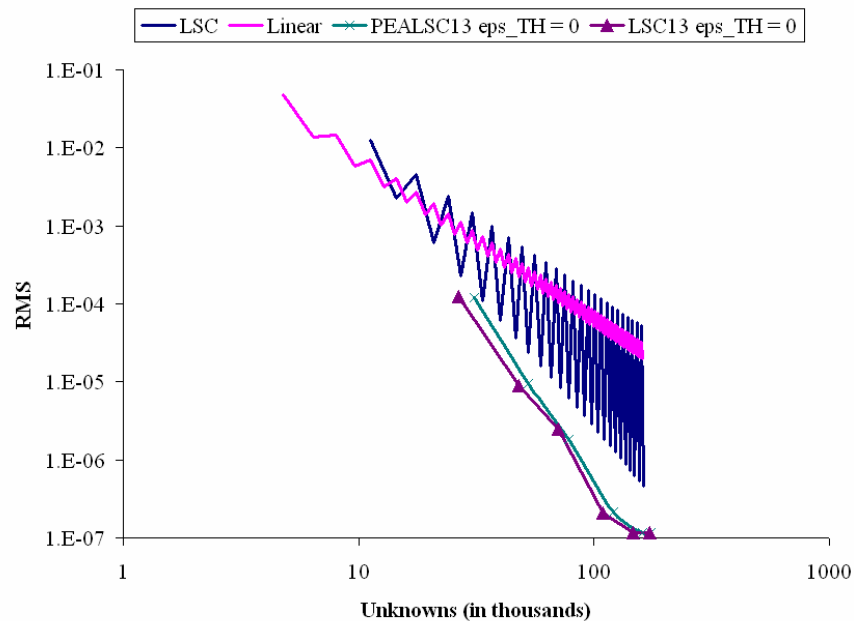
Figure 34   The RMS error in scalar fluxes from EQSP and Adaptive (LSC13 and PEALSC13) methods on the corner source problem.

Lastly, we plot exiting angular flux from various cells far away from the source as a function of azimuthal angle. These plots illustrate the ability of our adaptive methods (LSC is the only method shown for brevity; the others perform in a similar fashion) to interpolate the exiting angular flux. This interpolative ability is very important. If the exiting angular flux functions are not properly mapped the downstream angular flux will be wrong and will yield inaccurate results. Figure 35 shows the initial exiting angular flux functions using the LSC9 adaptive method. Figure 36 shows how the adaptive algorithm adds only the points that are needed to accurately interpolate the exiting angular flux.
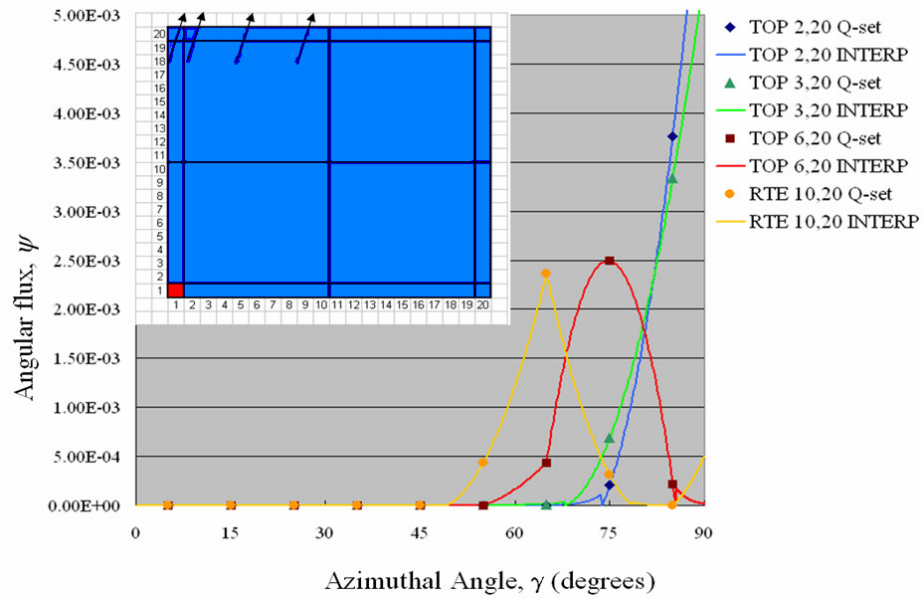
Figure 35   The exiting angular flux interpolated functions (at spatial positions noted by black arrows) before any refinements.
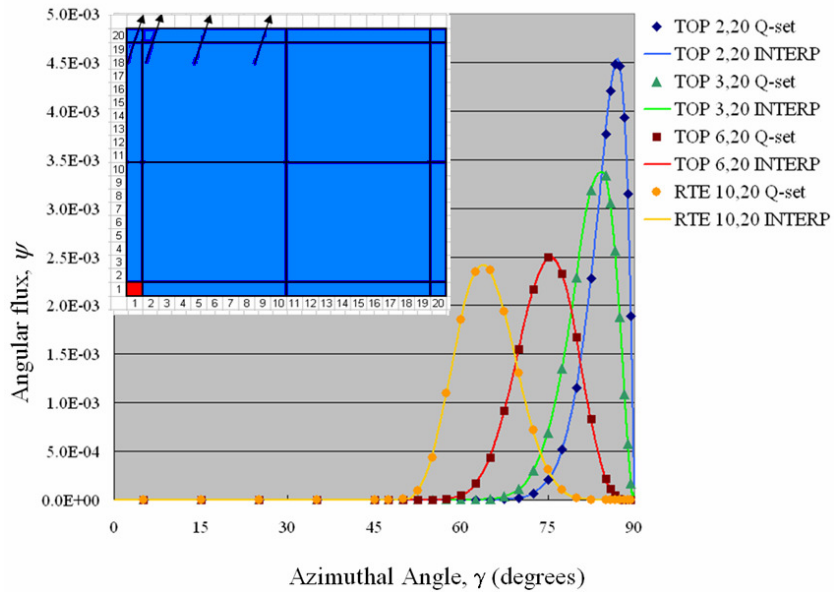

Figure 36   The exiting angular flux interpolated functions (at spatial positions noted by black arrows) after refinements.

G. Problems with Scattering Materials

It is a common misconception that scattering problems are immune to ray effects or that scattering somehow "smears" them away. Ray effects and other angular discretization errors are still present in problems with scattering. We examine a checker board problem (see Figure 37) designed to produce beams and shadows. A 2 cm by 2 cm isotropic source region (red) is placed at the center of a 20 cm by 20 cm problem with vacuum boundaries. The dark blue 2 cm by 2 cm square regions are purely absorbing ($\sigma_t = 100$ cm^{-1}) and the light blue regions have a scattering ratio of 0.5 ($\sigma_t = 1$ cm^{-1}). Each region is further subdivided into 1 mm by 1 mm cells, for a uniform 200 by 200 spatial grid.
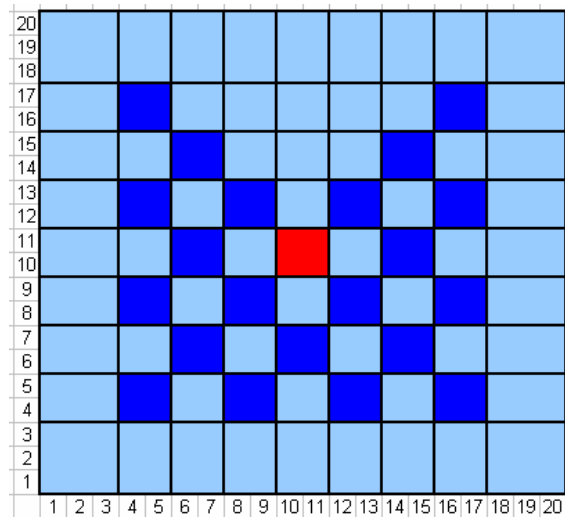
Figure 37 The checker board problem with a 2 cm by 2 cm isotropic source (red) placed at the center of a 20 cm by 20 cm problem with vacuum boundaries. The dark blue 2 cm by 2 cm squares are purely absorbing and the light blue areas have a scattering ratio of 0.5.

We use an LSC15 EQSP (2.4 million unknowns) and plot scalar flux vs. position on a 2D pseudo-color plane in Figure 38 to illustrate the ray effects that appear in this problem.

Figure 38   The solution of scalar flux for the checker board problem using LSC15 EQSP. The legend is the base-10 logarithm. The axes labels are in cm.

Figure 38 shows many rays, some of which are representative of the correct solution and some of which are artifacts. We can see the ray effects more clearly in Figure 39, where we plot the right edge scalar flux versus position along with a reference line that uses LSC2001 EQSP (320 million unknowns).
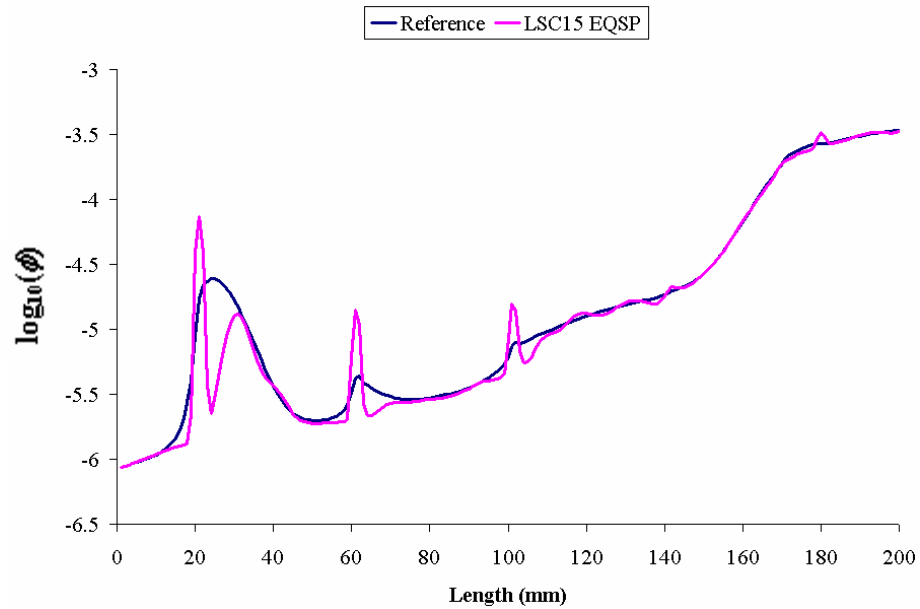
Figure 39   The right-edge scalar flux from LSC15 EQSP compared with a reference solution.

We perform the same tests using LSC9 adaptive method to eliminate the angular discretization errors and plot the results on a 2D pseudo-color plane in Figure 40. We use a threshold tolerance of 0.01% and an angular flux tolerance of 10%. Likewise we plot the right edge flux in Figure 41. The number of unknowns is 4.59 million and the RMS error in the scalar flux along the right edge is 3.19E-4.
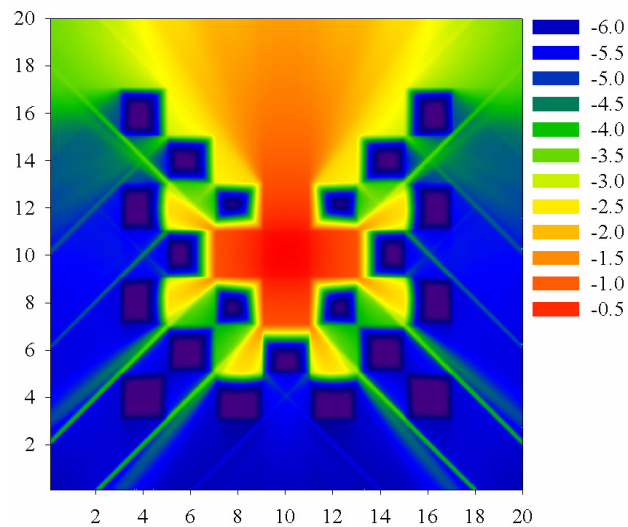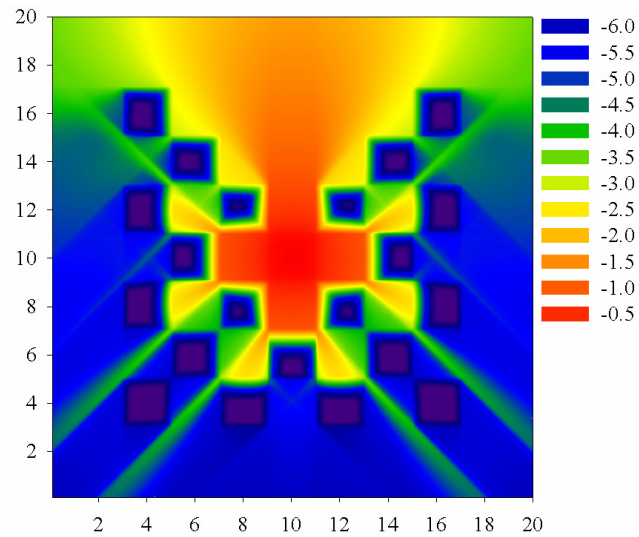
Figure 40   The solution of scalar flux for the checker board problem using LSC9. The legend is the base-10 logarithm. The axes labels are in cm.
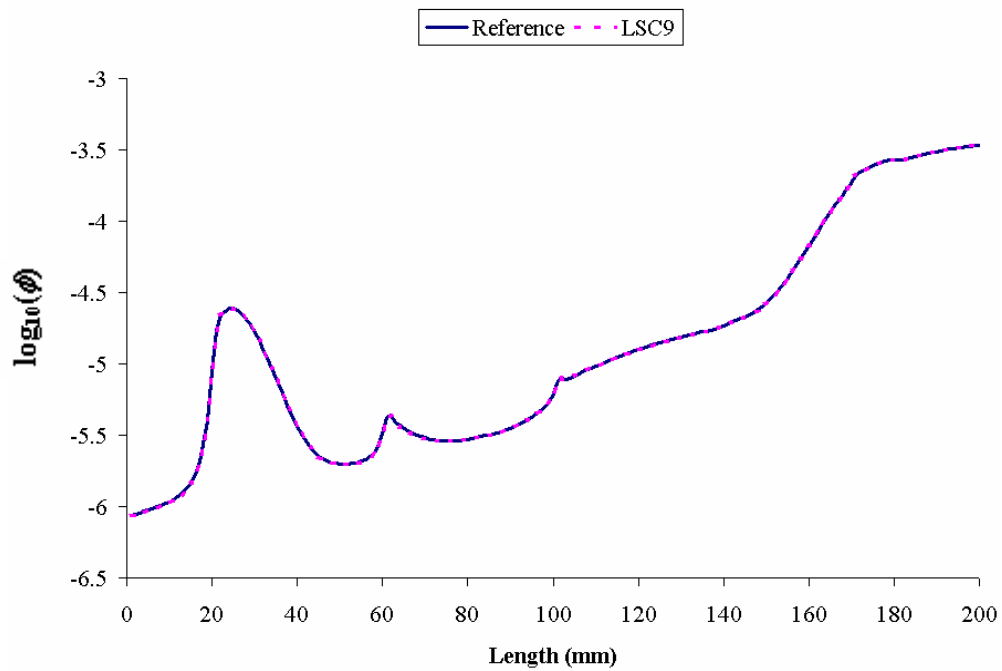
Figure 41   The right-edge scalar flux from LSC9 adaptive.

The adaptive methods produce a significant improvement. All ray effects have been eliminated as far as can be told from Figure 41. The edge scalar flux plot in Figure 41 is

even more impressive when one compares it to the size of an EQSP quadrature set needed to match this plot. To the naked eye there are no visible oscillations. In order to quantify the difference of accuracy between the EQSP LSC quadrature set and the LSC adaptive method we must use an EQSP LSC93 (14.9 million unknowns vs. 4.59 million for the adaptive) to achieve a comparable RMS error of 3.52E-4.

H. A "Point" Source Problem

In the previous problem we suspect that SC spatial anomalies are most likely producing artifacts along 45-degree lines because of square spatial cells. The triangular shaped areas of greater orange intensities on the other side of the purely absorbing regions are likely over valued and the collimated beam that should be visible in those scattering regions is completely smeared out. To illustrate this we have devised another scattering problem (see Figure 42) in which the regions are rectangular, but the cells remain square. As in the previous problem the red region is a square isotropic source but its size has been reduced to 1 mm. The dark blue regions are purely absorbing ($\sigma_t = 100$ cm^{-1}). The light blue regions have a scattering ratio of 0.5 ($\sigma_t = 1$ cm^{-1}). The regions are divided into 1 mm by 1 mm square cells.

Figure 42   The "point" source problem with rectangular shaped absorbing and scattering regions.

The shape of the rectangular cells is intended to force the collimated beams away from the $\pi/4$ directions. We apply our LSC9 adaptive method to the problem with a 10% interpolation tolerance and a 0.01% threshold tolerance and display the results in Figure 43.
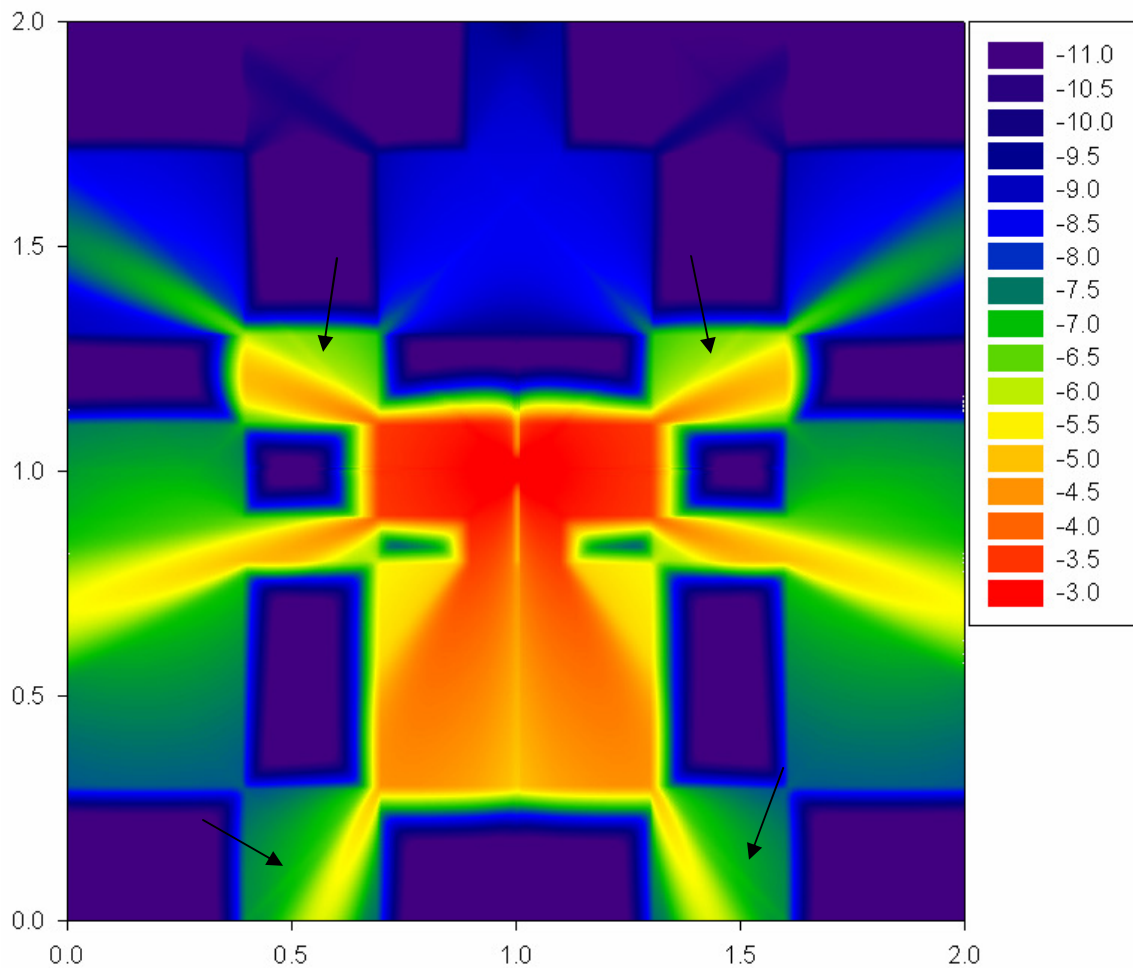
Figure 43   The scalar flux solution of the "point" source scattering problem with rectangular shaped regions. Axes units are decimeters.

The spatial anomalies due to the SC method are pointed to by the arrows. They are (barely visible) thin yellow lines ($10^{-5.5}$) at the odd multiples of $\pi/4$. A quick observation of the problem geometry unquestionably indicates that these irregularities are unphysical. We emphasize that these are not discrete-ordinate ray effects, but are artifacts of the spatial discretization.

I. Summary

In this section we presented numerical results from a variety of test problems. We employed several quadrature schemes including four adaptive schemes we have developed. We used simple one-dimensional function integration to illustrate basic properties of the various schemes, and then we turned to several two-dimensional transport problems. Results demonstrated that our adaptive schemes produce smaller solution errors with fewer unknowns than do standard schemes and that are methods do eliminate ray effects.

VI. CONCLUSION

A. Observations

We have presented our efforts toward an adaptive discrete-ordinates quadrature methodology, focusing on transport problems in two-dimensional Cartesian geometry. Our strategy involves several key components:

- A set of interpolatory functions that provide an interpolated solution at any value of the direction variables;

- Quadrature weights that are consistent with these interpolatory functions, in the sense that the quadrature sum of a function is equal to the exact integral of the interpolation through the quadrature points;

- Division of the spatial domain into "quadrature regions," each with its own adapting quadrature set;

- Refinement tests based on comparing evaluated functions against interpolated values;

- Refinement tests performed only on surfaces of quadrature regions, not on region or cell interiors.

Various methods in our strategic framework differ in their choices of initial sets, refinement-test points, and interpolatory functions.

Our results are encouraging. We have shown that it is possible to adapt quadrature sets to resolve local variations in angular fluxes, and we have shown that even very simple adaptation logic combined with very simple linear interpolation and trapezoidal-rule quadrature sets can achieve highly accurate solutions with relatively few unknowns. We have gone beyond this to a linear-in-cosines method that yields significantly improved accuracy with fewer unknowns. We have gone farther and developed a method that retains the ability to exactly integrate high-order polynomials in the direction cosines even given many levels of local adaptation.

Our main conclusion is bold and significant: Our adaptive discrete-ordinates strategy eliminates ray effects and other angular discretization errors to whatever tolerance the user specifies. It does so with far fewer unknowns than would be required by applying any quadrature set to the entire spatial domain. It also does so with far fewer unknowns than would be required by applying different "standard" quadrature sets in different spatial regions, without local refinement in angle.

An unexpected finding of our research was the ability of the EQSP LSC method to accurately integrate functions. In most cases (jump discontinuities are the exception) we observed a fourth-order convergence rate and more accurate integration than was provided by the Gauss-Chebyshev set with the same number of points. Even without adaptation, this LSC quadrature set appears to be worthy of further study.

Our proof of principle has laid the groundwork for a great deal of future research in the area of adaptive discrete ordinates methods. We offer our thoughts on this in the next section.

B. Future Work

Our study was restricted to two-dimensional Cartesian geometry, in which the angular flux varies in a complicated way in only the azimuthal direction. (Polar variations are smooth.) Thus, we focused on adaptive quadrature sets only for azimuthal-angle integration. In other coordinate systems, such as two-dimensional axisymmetric (r,z) and three-dimensional Cartesian, there can be complicated variations in both the polar and azimuthal directions. This will require significant extension of the ideas we have introduced here.

We have tested only refinement, not coarsening, of adaptive quadrature sets. We see coarsening as a simpler task, at least given our view that one should never try to get coarser than the "base" quadrature set, which means that coarsening steps are simply the undoing of previous refinement steps. We propose the same strategy as for refinement: compare an interpolated value at the candidate point against the calculated value. In the case of testing for coarsening, if the two are close enough then the quadrature point can be removed from the set. This strategy needs to be implemented and tested. We expect it to be most useful in time-dependent problems, in which the solution in a given spatial region can change significantly over time (and thus the quadrature set should as well).

In our work we have studied only isotropic scattering. Problems with strongly anisotropic scattering pose further challenges to the quadrature set, partly because there are more functions that must be accurately integrated to form an accurate scattering source. We believe that our methods that retain the high-order integration properties of the base quadrature set will perform well even with highly anisotropic scattering, but this

must be tested. The Linear method integrates the constant and the LSC method

integrates 0th and 1st order polynomials in $\sin^p(\gamma)$ and $\cos^q(\gamma)$. Strictly speaking, for

higher order spherical harmonics the Linear and LSC methods do not conserve; whereas

the PEA methods integrate higher orders to $p+q \leq N-1$.

There are other ways that should be considered for determination of the scalar flux.

Basing the adaptation on how the scalar flux is changing for the better as it is related to

some reaction rate (i.e. a physical quantity). Another approach that could be

implemented is a goal-oriented adaptive process. The adaptive process could be in terms

of a localized quantity of interest, where the related mathematical theory would

necessarily require the solution of an adjoint function.[31,32]

In our present implementations we take care to enforce particle conservation, and we

do so by ensuring that the exiting partial current from the surface of a region is exactly

the incident partial current on that surface of the neighboring region. In some

applications, the momentum carried by the particles and exchanged with the matter are

also important quantities to conserve. To enforce this in our framework will require that

we ensure continuity of second angular moments on surfaces in addition to the present

requirement of continuity of current (which is the first angular moment). Algorithms for

enforcing all necessary continuity conditions will need to be developed for these

applications.

In our work with interpolatory functions of higher order than linear, we found that

Gibb's phenomenon led to unlimited refinement at solution discontinuities. To prevent

this in our proof-of-principle code, we simply imposed a minimum spacing between quadrature points and did not permit further refinement. We believe that an interesting line of investigation would be to reduce the order of the interpolatory functions, ultimately down to linear, if a great deal of local refinement takes place. Linear interpolation is not subject to Gibb's phenomenon and thus should not lead to unlimited refinement.

In our work we employed what is often called "h-refinement," meaning that we fixed the order of the method and refined the spacing between points. An alternative is "p-refinement," in which the spacing of intervals is fixed and new degrees of freedom are devoted to higher-order methods. In the application of adaptive methods to differential equations, it is often the case that a combined "h-p-refinement" method is superior. It would be interesting, and likely fruitful, to develop such an approach for adaptive discrete ordinates.

REFERENCES

1.   B.G. Carlson and K.D. Lathrop, "Transport Theory – The Method of Discrete Ordinates," *Computing Methods in Reactor Physics,* Greenspan, Kelber and Okrent (eds.), Ch. 3, New York, (1968).

2.   J. F. Carew, K. Hu and G. Zamonsky, "Uniform Gauss-Weight Quadratures for Discrete Ordinate Transport Calculations," *Nuclear Science and Engineering,* **136**, 282-293, (2000).

3.   K. D. Lathrop, "Remedies for Ray Effects," *Nuclear Science and Engineering*, **45**, 255-268, (1971).

4.   E. E. Lewis and W. F. Miller, *Computational Methods of Neutron Transport,* John Wiley and Sons, Inc., New York, NY, (1993).

5.   R. C. Gast, "The Two-Dimensional Quadruple P_0 and P_1 Approximations," Report WARD-TM-274, Bettis Atomic Power Laboratory (1961).

6.   M. Natelson, "Variational Derivation of Discrete Ordinate-Like Approximations," *Nuclear Science and Engineering*, **43**, 131-144, (1971).

7.   J. Stepanek, "The DPN and QPN Surface Flux Integral Transport Method in One-Dimensional and X-Y Geometry," *Proc. ANS/ENS Int. Topical Meeting on Advances in Mathematical Methods for the Solution of Nuclear Engineering Problems,* April 27-29, 1981, Munich, Germany, European Nuclear Society (1981).

8.   L. L. Briggs, W. F. Miller and L. L. Lewis, "Ray Effect Mitigation in Discrete Ordinate-Like Angular Finite Element Approximations in Neutron Transport." *Nuclear Science and Engineering*, **57**, 205, (1975).

9.   P. N. Brown, B. Chang, "Locally Refined Quadrature Rules for S_N Transport," Report UCRL-JRNL-220755, Lawrence Livermore National Laboratory, (2006).

10.   G. Longoni and A. Haghighat, "Development and Application of the Regional Angular Refinement Technique and its Applications to Non-Conventional Problems," *Proc. PHYSOR 2002*, Seoul, Korea, Oct. 7-10, (2002).

11.   W. A. Rhoades and R. L. Childs, "The DORT Two-Dimensional Discrete Ordinates Transport Code," *Nuclear Science and Engineering*, **99**, 88-89, (1988).

12.   W. A. Rhoades and D. B. Simpson, "The TORT Three-Dimensional Discrete Ordinates Neutron/Photon (TORT version 3) Transport Code," Report ORNL/TM 13221, Oak Ridge National Laboratory, (1997).

13. T.R. Hill, "Efficient Methods for Time-Absorption (alpha) Eigenvalue Calculations," Report LA-9602-MS, Los Alamos, N.M, available from NTIS, (1983).

14. W. A. Rhoades, "The TORT Three-Dimensional Discrete Ordinates Neutron/Photon Ttransport Code," Report ORNL-6268, Oak Ridge National Laboratory, (1987).

15. R. E. Alcouffe, "Three Dimensional Transport Benchmark Exercise Using THREEDANT," Report LA-UR-90-3603, Los Alamos National Laboratory, (1990).

16. K. D. Lathrop, "Spatial Differencing of the Two-Dimensional Transport Equation," Report GA-8746, Gulf General Atomic (1968).

17. W. F. Walters, "The Relation Between Finite Element Methods and Nodal Methods in Transport Theory," *Progress in Nuclear Energy*, **18**, 21 (1986).

18. V. I. Krylov, *Approximate Calculations of Integrals*, Dover Publications, New York (2005).

19. Gwynne Evans, *Practical Numerical Integration*. Wiley, New York (1993).

20. B. G. Carlson and K. D. Lathrop, *Computing Methods in Reactor Physics*, Gordon and Breach, New York, (1968).

21. I. K. Abu-Shumays, "Compatible Product Angular Quadrature for Neutron Transport in x-y Geometry," *Nuclear Science and Engineering*, **64**, 299-316, (1977).

22. L. N. G. Filon, "On a Quadrature Formula for Trigonometric Integrals," *Proceedings Royal Society of Edinburgh,* **49**, 38-47, (1928).

23. G. Longoni and A. Haghighat, "Development of New Quadrature Sets with the Ordinate Splitting Technique", *Proceedings of the 2001 ANS International Meeting on Mathematical Methods for Nuclear Applications (M&C),* September 9-13, Salt Lake City, UT, (2001).

24. G. Longoni and A. Haghighat, "Development and Application of the Regional Angular Refinement Technique and Its Applications to Non-Conventional Problems," *Proc. PHYSOR*, Seoul, Korea, Oct. 7-10, (2002).

25. P.N. Brown, B. Chang, "Locally Refined Quadrature Rules for S_N Transport," UCRL-JRNL-220755, Lawrence Livermore National Laboratory, (2006).

26. Piessens, Doncker-Kapenga, Überhuber and Kahanr, *QUADPACK*, Springer-Verlag, Berlin, (1983).

27. A. S. Kronrod, *Nodes and Weights of Quadrature Formulae*, Consultants Bureau, New York, (1965).

28. I. K. Abu-Shumays, "Angular Quadratures for Improved Transport Computations," *Nuclear Science and Engineering*, **64**, 299 – 316 (1977).

29. J. R. Rice, "A Metalgorithm for Adaptive Quadrature," J. ACM, **22 (1)**, pages 61-82, January (1973).

30. I. K. Abu-Shumays, "Angular Quadratures for Improved Transport Computations," *Transport Theory and Statistical Physics*, **30 (2&3)**, 169 – 204 (2001).

31. Yaqi Wang, Jean C. Ragusa, "Goal-Oriented hp-Mesh Adaptation for the 1-D Multigroup Diffusion Equations," *Proceedings of the ANS Mathematics, Computations and Supercomputing in Nuclear Applications (M&C-SNA 2007) International Conference*, April 15-19, Monterey, CA., (2007).

32. Yaqi Wang, Jean C. Ragusa, "Standard hp- and Goal-Oriented hp-Mesh Adaptation for Multigroup Diffusion Equations," submitted to *Nuclear Science and Engineering*, (2007).

APPENDIX A. STEP CHARACTERISTIC FORMULAS

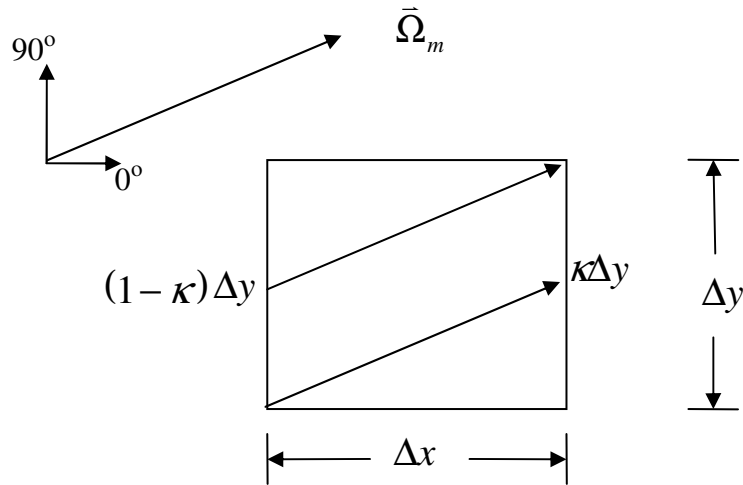**Problem Overview and Definitions**

Figure 44   A rectangular cell drawn with characteristic lines entering through the left (L) and bottom (B) edges and exiting through the top (T) and right (R) edges.

The one-speed, steady-state Boltzmann transport equation discretized in the direction cosine variables, $\mu_m = \bar{\Omega}_m \cdot \bar{e}_x$ and $\eta_m = \bar{\Omega}_m \cdot \bar{e}_y$ in two-dimensional Cartesian geometry is:

$$\left[\mu_m \frac{\partial}{\partial x} + \eta_m \frac{\partial}{\partial y} + \Sigma_t(x, y) \right] \psi_m(x, y) = Q(x, y) \tag{A1}$$

The source term includes embedded emitters that are independent of the flux as well as the scattering source:

$$Q(x,y) = \frac{1}{4\pi}\left[Q_{ext}(x,y) + \Sigma_s(x,y)\phi(x,y)\right] \tag{A2}$$

For clarity of derivation, we consider only isotropic emitters and scattering. The scalar flux, ϕ is solved using the discrete ordinates approximation:

$$\phi(x,y) \equiv \sum_{\tilde{m}=1}^{M} w_{\tilde{m}}\psi_{\tilde{m}}(x,y), \tag{A3}$$

where the quadrature rule employed has M quadrature directions $\{\mu_m, \eta_m\}$ and weights, $\{w_m\}$.

The cell optical thickness is defined in the x and y directions respectively as:

$$\tau_x = \frac{\Sigma_t \Delta x}{\mu} \quad \text{and} \quad \tau_y = \frac{\Sigma_t \Delta y}{\eta} \tag{A4}$$

The ratio of the x to the y optical thickness is:

$$\kappa = \frac{\eta \Delta x}{\mu \Delta y} = \frac{\tau_x}{\tau_y} \tag{A5}$$

The exponential moment functions are:

$$M_n(x) \equiv \int_0^1 dt\, (1-t)^n\, e^{-xt} \tag{A6}$$

$$M_0(x) = \frac{1-e^{-x}}{x} \tag{A7}$$

$$M_1(x) = \frac{1-M_0(x)}{x} \tag{A8}$$

Consider $\mu_m > 0$ and $\eta_m > 0$. If the flux entering the bottom edge of the cell is

constant (ψ_B), then the resulting flux in the cell is:

$$\psi_B(x,y) = \begin{cases} \psi_B e^{\left(-\frac{\Sigma_t y}{\eta}\right)} & \dfrac{x}{\mu} \geq \dfrac{y}{\eta} \\ 0 & \text{otherwise} \end{cases} \tag{A9}$$

If the flux entering the left edge of the cell is constant (ψ_L), then the resulting flux in

the cell is:

$$\psi_L(x,y) = \begin{cases} \psi_L e^{\left(-\frac{\Sigma_t x}{\mu}\right)} & \dfrac{x}{\mu} \le \dfrac{y}{\eta} \\ 0 & \text{otherwise} \end{cases} \tag{A10}$$

The flux resulting from a constant volumetric source is:

$$\psi_S(x,y) = \begin{cases} \displaystyle\int_0^x \dfrac{dx'}{\mu} Q e^{\left(-\Sigma_t \frac{x-x'}{\mu}\right)} & \dfrac{x}{\mu} \le \dfrac{y}{\eta} \\ \displaystyle\int_0^y \dfrac{dy'}{\eta} Q e^{\left(-\Sigma_t \frac{y-y'}{\eta}\right)} & \dfrac{x}{\mu} \ge \dfrac{y}{\eta} \end{cases} \tag{A11}$$

Derivations

The case examined here is in the first quadrant ($\mu > 0$ and $\eta > 0$) where $\kappa < 1$. The case where $\kappa > 1$ accomplished by flipping the variables for the exiting surfaces. Other quadrants are handled with sign reversals of μ or η where appropriate. The flux exiting through the top edge is a combination of the flux contributions from the left face and the source:

$$\psi_T = \psi_{TL} + \psi_{TS} \tag{A12}$$

The flux through the top due to the left edge is:

$$\psi_{TL} = \frac{1}{\Delta x}\psi_L \int\limits_0^{\Delta x} e^{-\frac{\Sigma_t}{\mu}x}\,dx \tag{A13}$$

We use the following change of variables:

$$v = \frac{x}{\Delta x} \quad dv = \frac{dx}{\Delta x} \tag{A14}$$

$$\psi_{TL} = \psi_L \int\limits_0^1 e^{-\tau_x v}\,dv = \psi_L M_0(\tau_x) \tag{A15}$$

The flux emitted from the source through the top edge is:

$$\psi_{TS} = \frac{1}{\Delta x}\int\limits_0^{\Delta x}\frac{Q}{\mu}\int\limits_0^x e^{\left(-\Sigma_t\frac{x-\tilde{x}}{\mu}\right)}\,d\tilde{x}\,dx \tag{A16}$$

We use the following change of variables:

$$v = \frac{x}{\Delta x} \quad \tilde{v} = \frac{\tilde{x}}{\Delta\tilde{x}} \tag{A17}$$

$$\psi_{TS} = \frac{Q}{\mu}\int\limits_0^1 e^{-\tau_x v}\int\limits_0^v e^{\tau_x\tilde{v}}\,d\tilde{v}\,dv = \frac{Q}{\Sigma_t}\left[1 - M_0(\tau_x)\right] \tag{A18}$$

The flux exiting through the top is then:

$$\boxed{\psi_T = \psi_L M_0(\tau_x) + \frac{Q}{\Sigma_t}\left[1 - M_0(\tau_x)\right]} \qquad \text{(A19)}$$

The flux exiting through the right edge is a combination of the flux contributions from the left face, the bottom face and the source:

$$\psi_R = \psi_{RB} + \psi_{RL} + \psi_{RS} \qquad \text{(A20)}$$

The flux exiting through the right due to the bottom edge is:

$$\psi_{RB} = \frac{1}{\Delta y}\psi_B \int_0^{\kappa\Delta y} e^{-\frac{\Sigma_t}{\eta}y}\,dy \qquad \text{(A21)}$$

We use the following change of variables:

$$v = \frac{y}{\kappa\Delta y} \quad \text{and} \quad dv = \frac{dy}{\kappa\Delta y} \qquad \text{(A22)}$$

$$\psi_{RB} = \frac{1}{\Delta y}\psi_B \int_0^1 e^{-\frac{\Sigma_t}{\eta}\kappa\Delta y v}\,\kappa\Delta y\,dv = \psi_B \int_0^1 e^{-\tau_x v}\kappa\,dv = \kappa\psi_B M_0(\tau_x) \qquad \text{(A23)}$$

The flux exiting through the right due to the left edge is:

$$\psi_{RL} = \frac{1}{\Delta y}\psi_L e^{-\tau_x}\int\limits_{\kappa\Delta y}^{\Delta y} dy = \frac{1}{\Delta y}\psi_L e^{-\tau_x}\left(\Delta y - \kappa\Delta y\right) = \left(1-\kappa\right)\psi_L e^{-\tau_x} \qquad (A24)$$

The flux emitted from the volumetric source through the right edge is:

$$\psi_{RS} = \frac{1}{\Delta y}Q\int\limits_0^{\kappa\Delta y} dy\int\limits_0^y \frac{d\tilde{y}}{\eta}e^{\left(-\Sigma_t\frac{y-\tilde{y}}{\eta}\right)} + \frac{1}{\Delta y}Q\int\limits_{\kappa\Delta y}^{\Delta y} dy\int\limits_0^{\Delta x}\frac{d\tilde{x}}{\mu}e^{\left(-\Sigma_t\frac{\Delta x-\tilde{x}}{\mu}\right)} \qquad (A25)$$

$$\psi_{RS} = \frac{1}{\Delta y\eta}Q\int\limits_0^{\kappa\Delta y} dy e^{\left(-\frac{\Sigma_t}{\eta}y\right)}\int\limits_0^y e^{\left(\frac{\Sigma_t}{\eta}\tilde{y}\right)}d\tilde{y} + \frac{1}{\Delta y\mu}Qe^{-\tau_x}\int\limits_{\kappa\Delta y}^{\Delta y} dy\int\limits_0^{\Delta x} d\tilde{x}e^{\left(\frac{\Sigma_t}{\mu}\tilde{x}\right)} \qquad (A26)$$

We use the following change in variables:

$$v = \frac{y}{\kappa\Delta y} \quad dv = \frac{dy}{\kappa\Delta y} \quad \tilde{v} = \frac{\tilde{y}}{\kappa\Delta y} \quad d\tilde{v} = \frac{d\tilde{y}}{\kappa\Delta y} \quad \tilde{u} = \frac{\tilde{x}}{\Delta x} \quad d\tilde{u} = \frac{d\tilde{x}}{\Delta x} \qquad (A27)$$

$$\psi_{RS} = \frac{1}{\Delta y\eta}\kappa\Delta y\kappa\Delta yS\int\limits_0^1 dv e^{(-\tau_x v)}\int\limits_0^v d\tilde{v}e^{(\tau_x\tilde{v})} + \frac{\Delta x}{\Delta y\mu}Qe^{-\tau_x}\int\limits_{\kappa\Delta y}^{\Delta y} dy\int\limits_0^1 e^{(\tau_x\tilde{u})}d\tilde{u} \qquad (A28)$$

$$\psi_{TS} = \frac{1}{\Delta y \eta} \kappa \Delta y \kappa \Delta y \frac{1}{\tau_x} Q \int_0^1 \left(1 - e^{-\tau_x v}\right) dv + \frac{\Delta x}{\Delta y \mu \tau_x} S \int_{\kappa \Delta y}^{\Delta y} \left(1 - e^{-\tau_x}\right) dy \qquad \text{(A29)}$$

$$\psi_{TS} = Q \frac{\Delta x}{\mu} \left(\kappa M_1(\tau_x) + (1 - \kappa) M_0(\tau_x)\right) \qquad \text{(A30)}$$

The flux exiting through the right is then:

$$\boxed{\psi_R = \kappa \psi_B M_0(\tau_x) + (1 - \kappa) \psi_L e^{-\tau_x} + Q \left(\kappa \frac{\Delta x}{\mu} M_1(\tau_x) + (1 - \kappa) \frac{\Delta x}{\mu} M_0(\tau_x)\right)} \quad \text{(A31)}$$

VITA

Joseph Carlyle Stone served as a nuclear trained electrical operator onboard the USS Sand Lance from 1991 until 1995. He received his Bachelor of Science degree in nuclear engineering from Texas A&M University in 1999. He entered the graduate studies program in the Nuclear Engineering Department at Texas A&M University in January, 2000 and received his Master of Science degree in December 2001. He met his wife while an undergraduate at Texas A&M. They were married in 2000. They have two children and are planning for more. He completed his Doctor of Philosophy in December of 2007. He and his family moved to Pittsburgh, PA., where he accepted a position as an engineer at Bettis Atomic Power Laboratory.

Dr. Stone may be reached at:

1615 California Ave.

White Oak, PA 15131

hapstone@tamu.edu